A Two-Dimensional Radiation–Turbulence Climate Model. I: Sensitivity to Cirrus Radiative Properties

SZU-CHENG S. OU AND KUO-NAN LIOU

Department of Meteorology, University of Utah, Salt Lake City, UT 84112

(Manuscript received 3 October 1983, in final form 5 June 1984)

ABSTRACT

Based on the thermodynamic energy balance between radiation and vertical plus horizontal dynamic transports, a two-dimensional radiation–turbulence climate model is developed. This model consists of a broadband solar and IR radiation transfer scheme previously presented by the authors and vertical and horizontal dynamic eddy transports utilizing the elementary turbulent theory. In the model, three kinds of feedback mechanisms are considered: the humidity feedback via the constant relative humidity assumption, the ice–albedo feedback via a preliminary correlation between the surface albedo and the surface temperature and the dynamic transport feedback through the parameterization of eddy transports and the prescribed mean wind field. A standard temperature field, which differs from the climatological data by no more than 0.1°C, is first obtained by solving the coupled thermodynamic and surface flux budget equations using climatological distributions of H_2O, CO_2, O_3, surface albedo and cloud properties. The model-derived atmospheric radiation budget, surface energy balance and horizontal transport patterns compare reasonably well with available observational data. Further validation of the model includes sensitivity studies on the effects of doubling of CO_2 and a 2% increase in the solar constant. The temperature changes relative to the standard field on these experiments agree closely with those presented by Manabe and Wetherald utilizing a general circulation model. To investigate the two-dimensional cirrus–radiation interaction, a relationship between the cirrus IR emissivity and solar reflectance (and transmittance) is established based on the parameterization equations. On the basis of a number of experiments involving various couplings and feedbacks, we find that 1) the humidity and albedo feedbacks are most active in the tropics and arctic area, respectively, 2) the dynamic transport is a negative feedback in the equatorial and polar regions but a positive one in midlatitudes and 3) the relative importance of each feedback depends only slightly on the radiative properties of cirrus. Finally, we demonstrate that slight variations in the cirrus IR emissivity lead to significant temperature perturbations in the arctic surface and tropical troposphere.

1. Introduction

Clouds regularly occupy about 50% of the sky over a global scale and have been recognized to be the most important regulators of the radiation balance of the earth–atmosphere system. On the one hand, clouds reflect a significant portion of incoming solar fluxes. On the other, clouds also trap the outgoing thermal infrared fluxes emitted from the earth's surface and lower troposphere. The competition of the so-called solar albedo effect versus the IR greenhouse effect determines whether the earth–atmosphere system will gain or lose radiative energy during a specific climate change which leads to warming or cooling of the system. The local cloud albedo and greenhouse effects obviously depend on the specific atmosphere and earth conditions under which the clouds are embedded and on the geometrical and physical composition of the clouds. In addition, various feedback mechanisms such as the humidity, coverage of ice–snow, and dynamic transport when coupled with clouds, also affect the thermodynamic equilibrium of the atmosphere in an intricate way.

In recent years, a number of studies have been focused on the subject of the cloud–radiation interaction. Utilizing radiation budget data derived from satellites, Hartmann and Short (1980), Herman *et al.* (1980) and Ohring and Clapp (1980) have attempted to determine the relative importance of the solar albedo and IR greenhouse effects due to the presence of clouds. While these analyses illustrate that the solar albedo effect is greater than the IR greenhouse effect at the top of the atmosphere with respect to variations in the fractional cloud coverage, the degree and extent to which these two affect the thermal structure of the earth–atmosphere system have not been quantified. Climate sensitivity due to cloud cover variations has also been performed by Wetherald and Manabe (1980) using a general circulation model. Moreover, numerous theoretical investigations employing one-dimensional radiative–convective models have been carried out to understand the effects of feedbacks on the interactions of clouds and some aspects of dynamic processes in terms of parameterizations between cloud variables and temperature or humidity (Paltridge, 1980; Wang *et al.*, 1981; Stephens

and Webster, 1981; Charlock, 1982). The fundamental issues to be resolved appear to be 1) the quantitative influence of the albedo and greenhouse effects on the thermal structure of the earth–atmosphere system due to the presence of various types of clouds and 2) the effects of various feedbacks on cloud–radiation and cloud–dynamic interactions. It would seem that a two-dimensional statistical–dynamical climate model is particularly suitable for understanding some aspects of the interactions of cloud–radiation and dynamic processes, since the latitudinal dependence of various physical processes can be accounted for and understood quantitatively.

In this paper, we wish to propose a two-dimensional climate model based on parameterizations of solar and IR radiation transfer as well as vertical and horizontal dynamic transports. Two-dimensional climate modeling has been undertaken by Potter *et al.* (1978) who have presented some simulation results for their model performance. However, details of radiation and dynamic parameterizations in their model have not been presented in the literature. In a more recent publication, Peng *et al.* (1982) described a two-dimensional climate model which was intended for the study of the thermal response to climate changes due to doubling of CO_2 and solar constant variations (Chou *et al.*, 1982). The present two-dimensional climate model is constructed specifically for investigations of the interactions of cloud–radiation and dynamic processes. It is a logical extension of the semi-two-dimensional radiation–turbulent model developed previously by Liou and Ou (1983). The approach is therefore based on the concept of thermodynamic energy balance in which parameterizations of dynamic transports are carried out in harmony with this balance. As we proceed with the presentation of various dynamic parameterizations we shall describe, whenever appropriate, differences between these parameterizations and those provided in the aforementioned pioneering papers.

Section 2 of this paper describes the development of a two-dimensional climate model on the basis of the thermodynamic energy balance. Parameterizations of vertical and large-scale horizontal transports are then presented in Section 3 in which the eddy fluxes are parameterized in terms of the basic K-theory for turbulent transports. In addition, parameterizations of humidity, ice–albedo and dynamic transport feedbacks in the context of the two-dimensional climate model are mathematically and physically discussed in Section 4, and in Section 5, we present numerical solutions to model climatic perturbations. Model simulation results including the radiation budget at the top of the atmosphere, surface energy balance and dynamic transport pattern are illustrated in Section 6 and are compared with available observational and statistical data. Thermal responses produced by variations in cirrus radiation properties are subsequently analyzed in Section 7 in terms of the competition of the solar albedo and IR greenhouse effects and various feedback mechanisms. Finally, in light of the model performance and sensitivity analysis, conclusions are given in Section 8.

2. Development of a two-dimensional thermodynamic model

Consider a three-dimensional (x, y, z) parcel of air in an incompressible flow at a specific time t. The thermodynamic energy sources and sinks for such a parcel of air are 1) the internal energy U associated with the temperature, 2) the potential energy ϕ in the gravitational field, 3) the work done by the system W and 4) the latent heat transition Lq due to condensation or evaporation where L denotes the latent heat per unit mass and q is the mixing ratio. These energy sources and sinks must be balanced by the radiative heat energy exchanges due to solar and thermal infrared radiation transfer.

Let the total static energy per unit mass in (x, y, z, t) coordinates be denoted as

$$E = U + \Phi + W + Lq. \tag{2.1}$$

Then we find upon using the equation of continuity in an incompressible flow $\nabla \cdot \mathbf{V} = 0$ that

$$\frac{d}{dt}(\rho E) = \frac{\partial}{\partial t}(\rho E) + \nabla \cdot \mathbf{V}E = -\nabla \cdot \mathbf{F}, \tag{2.2}$$

where ρ is the air density and $\mathbf{F}$ is the three-dimensional radiative flux density. The internal energy $U = C_v T$ where C_v is the specific heat at constant volume, while the work done by the system $W = R_m T$ where R_m is the individual constant for air. Thus, $U + W = (C_v + R_m)T = C_p T$ with C_p the specific heat at constant pressure. We also note that the potential energy is a function of height (z) only, so that we write $\Phi = \Phi_z = gz$. It follows that $E = C_p T + \Phi_z + Lq$.

After carrying out temporal and zonal averaged procedures we find

$$\frac{\partial}{\partial t}\rho\{C_p[\bar{T}] + L[\bar{q}]\} + \frac{\partial}{\partial z}\rho\{[\bar{w}][\bar{E}] + [\bar{w}^*\bar{E}^*] + [\overline{w'E'}]\} + \frac{1}{a\cos\lambda}\frac{\partial}{\partial \lambda}\cos\lambda\rho\{[\bar{v}][\bar{E}][\overline{v'E'}] + [\bar{v}^*\bar{E}^*]\} = -\frac{\partial F}{\partial z}, \tag{2.3}$$

where λ and a denote the latitude and earth mean radius respectively. The terms $[\bar{v}][\bar{E}]$, $[\bar{v}^*\bar{E}^*]$ and $[\overline{v'E'}]$ represent the transport of moist static energy by mean flow, stationary eddy and transient eddy in the meridional direction respectively. Likewise, $[\bar{w}][\bar{E}]$, $[\bar{w}^*\bar{E}^*]$ and $[\overline{w'E'}]$ represent their counterparts in

the vertical direction. Moreover, we define the vertical and horizontal transport fluxes in the form

$$F_v = \rho\{[\bar{w}][\bar{E}] + [\bar{w}^*\bar{E}^*] + [\overline{w'E'}]\},$$
$$F_h = \rho\{[\bar{v}][\bar{E}] + [\bar{v}^*\bar{E}^*] + [\overline{v'E'}]\}. \quad (2.4)$$

This leads to the simplification of Eq. (2.3) in the form

$$-\frac{\partial}{\partial t}\rho\{C_p[\bar{T}] + L[\bar{q}]\} = \frac{\partial}{\partial z}F_v + \frac{1}{a\cos\lambda}\frac{\partial}{\partial\lambda}\cos\lambda F_h + \frac{\partial F}{\partial z}. \quad (2.5)$$

To obtain the equilibrium temperature in a two-dimensional (z, λ) domain, we first set the local time rate of change of temperature and humidity equal to zero for steady state conditions. We then perform integration in the z-direction using Eqs. (2.3) and (2.4) to obtain

$$F_v(z, \lambda) - F_v(0, \lambda) + \frac{1}{a\cos\lambda}\frac{\partial}{\partial\lambda}\cos\lambda\int_0^z F_h(z', \lambda)dz' = F(0, \lambda) - F(z, \lambda). \quad (2.6)$$

The surface term (i.e., $z = 0$) is defined in the form

$$-R(0, \lambda) = F(0, \lambda) + F_v(0, \lambda). \quad (2.7)$$

Here the surface term is the balance of net radiative and vertical fluxes at the surface. Thus, (2.6) may be rewritten in the form

$$F_v(z, \lambda) + \frac{1}{a\cos\lambda}\frac{\partial}{\partial\lambda}\cos\lambda\int_0^z F_h(z', \lambda)dz' = -F(z, \lambda) - R(0, \lambda). \quad (2.8)$$

This equation represents the energy balance of an infinitesimal column of air below a height z and at a latitude λ. At the surface and height z, the gain or loss of energy is due to net radiative and vertical fluxes. The integral term denotes the integrated large-scale horizontal flux along the latitude which is normally poleward. Each term in Eq. (2.8) implicitly depends on the temperature and humidity distributions from both radiative and dynamic points of view. Equations (2.7) and (2.8) form the basis of a two-dimensional thermodynamic model. In order to compute the temperature field due to perturbations of various atmospheric components and feedbacks, it is necessary to simplify each term in terms of physical and numerical parameterizations. Parameterizations of IR and solar radiative flux transfer in clear and cloudy atmospheres have been rather comprehensively reported in our previous publications and shall not be duplicated here. However, parameterizations of vertical and horizontal eddy transports require the use of the elementary turbulent theory and available large-scale data base, in line with the two-dimensional climate model. In the following section, we present the manner in which these parameterizations are carried out.

3. Parameterizations of dynamic transports

a. *Vertical transport*

As illustrated in Eq. (2.4), the vertical transport consists of contributions due to the mean flow, transient eddy and stationary eddy. The stationary eddy is physically a very small quantity (Oort and Rasmusson, 1971) and for all practical purposes it may be ignored. The mean flow term depends on the vertical velocity which will be prescribed by utilizing the annual zonal data computed by Oort and Rasmusson. Moreover, we shall assume in this model that the relative humidity is constant (Manabe and Wetherald, 1967). As shown in the paper by Liou and Ou (1983), the vertical transient eddy may be parameterized in the form

$$\rho[\overline{w'E'}] = -k_z\rho C_p\left(\frac{\partial T}{\partial z} + \gamma'\right), \quad (3.1)$$

where the modified moist adiabatic lapse rate is defined by

$$\gamma' = \gamma_d + \frac{L}{C_p}\frac{\partial q}{\partial z} - \gamma_c. \quad (3.2)$$

In Eq. (3.2), γ_d is the dry adiabatic lapse rate and we add a term γ_c, which is known as the countergradient lapse rate (Deardorff, 1972). Analyses of the climatological temperature and humidity profiles presented by Oort and Rasmusson (1971) reveal that the atmosphere near the ground is mostly stable (i.e., $[\overline{w'E'}] \leq 0$). However, observed data derived by Budyko (1982) show that there are upward eddy fluxes near the ground for almost all latitudes. This inconsistency has been discussed by a number of boundary layer researchers. Deardorff (1966), for example, proposed a factor γ_c to be subtracted from the term $(\partial T/\partial z + \gamma_d)$. Considering a time scale of several hours and an area of about 10×10 km^2, he obtained a value of 0.7°C km^{-1}. Later, Deardorff (1972) derived a theoretical expression for γ_c which is given by $(g\overline{\theta'^2})/(\theta_0\overline{w'^2})$ where θ_0 is the average potential temperature in the boundary layer, g the gravitational acceleration, and $\overline{\theta'^2}$ and $\overline{w'^2}$ the time variance of the potential temperature and vertical velocity respectively. For a sufficiently long-time average, Deardorff suggested an order of two for the γ_c value that he derived empirically. In a more recent paper by Saltzman and Ashe (1976), a γ_c value of 5°C km^{-1} for the Northern Hemisphere and a time scale of a month was utilized in their climate modeling studies. Since $\overline{\theta'^2}$ and $\overline{w'^2}$ depend on complicated atmospheric scenarios, it is evident that γ_c is subject to great variations. We found that the countergradient

lapse rate should be on the order of $\sim 10°C\ km^{-1}$ for our steady-state climate models and feedback studies.

The foregoing parameterization of the vertical transient eddy includes contributions of large-scale and small-scale eddies in an approximate way. In the two-dimensional climate model presented by Peng *et al.* (1982), however, the vertical transient eddy was divided into two separate parts. The large-scale component was related to the large-scale horizontal eddy transport by a constant factor which was determined from the baroclinic instability theory with a β-effect adjustment. The small-scale part was determined by the K-theory discussed here and in Liou and Ou (1983). Based on the boundary layer theory (O'Brien, 1970), the vertical eddy transport coefficient due to small-scale eddy vanishes at the top of the Ekman layer (~ 2 km). Moreover, in a parameterization study associated with GCM, Branscome (1983) showed that there is a maximum in the vertical sensible heat flux near ~ 2 km. Thus, it appears that the small-scale eddy should be confined within the Ekman layer and that the large-scale eddy should be responsible for transport in the free atmosphere. The manner in which we combine small-scale and large-scale vertical eddies using the K-theory in turbulence appears to be in harmony with the parameterization principle for climate modeling from the viewpoint of the thermodynamic energy balance approach.

b. Horizontal transport

The large-scale horizontal flux [Eq. (2.4)] again is composed of contributions from the mean flow, transient eddy and stationary eddy. The mean meridional wind velocity is prescribed using the data computed by Oort and Rasmusson for v and w components. This implies that mean meridional and Hadley circulations are fixed in climatic perturbations. Transient and stationary eddy transports, however, are parameterized, and are allowed to vary with temperature and humidity gradients.

Many attempts have been made in the last two decades to correlate the large-scale horizontal eddy flux of sensible heat with the temperature gradient (see, e.g., Clapp, 1970). Clapp proposed that the meridional transient eddy sensible heat flux may be expressed by

$$[\overline{v'T'}] = -K\partial T/\partial\lambda. \tag{3.3}$$

He further suggested that the proportional constant K should be a function of the temperature gradient so that, in effect, $[\overline{v'T'}]$ varies with the temperature gradient to the second power. Utilizing a harmonic analysis, Srivatsangam (1978) found that the best correlation could be obtained between the eddy sensible heat flux and the temperature gradient, if the former is evaluated at about 50°N, and the latter is obtained by finite differences between 20 and 80°N. Lorenz (1979) concluded that Eq. (3.3) is physically valid only for long-term time averages and seasonal variations of the largest spatial scale. More recently, Stone and Miller (1980) performed statistical correlations between heat fluxes and temperature gradients employing month-to-month data of transient and stationary eddy fluxes and temperatures compiled by Oort and Rasmusson. In their study, surface and vertically averaged temperature gradients were adopted for correlation analyses. They illustrated that the sum of transient and stationary eddy sensible heat fluxes correlate well with the mean temperature gradient, with correlation coefficients $\geqslant 82.3\%$ for latitudes between 30 and 60°N. Also, they found that the correlation is best at 30°N and deteriorates poleward. In addition to the aforementioned studies based on the turbulence theory for the parameterization of large-scale horizontal eddy transports of sensible heat, numerous attempts have been made to parameterize the eddy transport based on the baroclinic instability theory (e.g., Green, 1970; Stone, 1974; Sasamori, 1978a,b; and Branscome, 1983). From this dynamic approach, however, effects of radiative heating and latent heat release were not properly accounted for in the parameterization process. Consequently, it is not clear whether such a dynamic parameterization is physically adequate for and consistent with simplified climate models and feedback studies in which temperature and humidity fields (not wind fields) are the prime model variables.

In view of the above discussions and reviews and consistent with the present steady-state two-dimensional climate model, we have followed the K-theory in association with available data to parameterize the large-scale horizontal transport. We postulate that the integrated eddy heat fluxes may be correlated with the integrated temperature gradient such that

$$\int_0^z ([\overline{v'T'}] + [\bar{v}^*\bar{T}^*])\rho dz' = -K_1 \int_0^z \left(\frac{\partial T}{\partial\lambda} + K_2\right)\rho dz'. \tag{3.4}$$

Although K_2 denoted in Eq. (3.4) has no specific physical meaning, it allows a better correlation to be established for the large-scale flow in the context of a climatic time scale. This K_2 factor was incorporated in the analysis of Stone and Miller (1980). In the climatic sense, K_2 is similar to the countergradient lapse rate associated with the vertical transient eddy flux defined previously. In order to test the validity of Eq. (3.4), we have carried out statistical analyses using monthly data sets of $[\overline{v'T'}] + [\bar{v}^*\bar{T}^*]$ and temperature presented by Oort and Rasmusson. Fig. 1 depicts the coefficient of correlation as a function of the latitude for a number of pressure levels. As shown, negative and poor correlations are seen in latitudes below about 20°N. However, between 20 and 60°N, the coefficients of correlation are greater

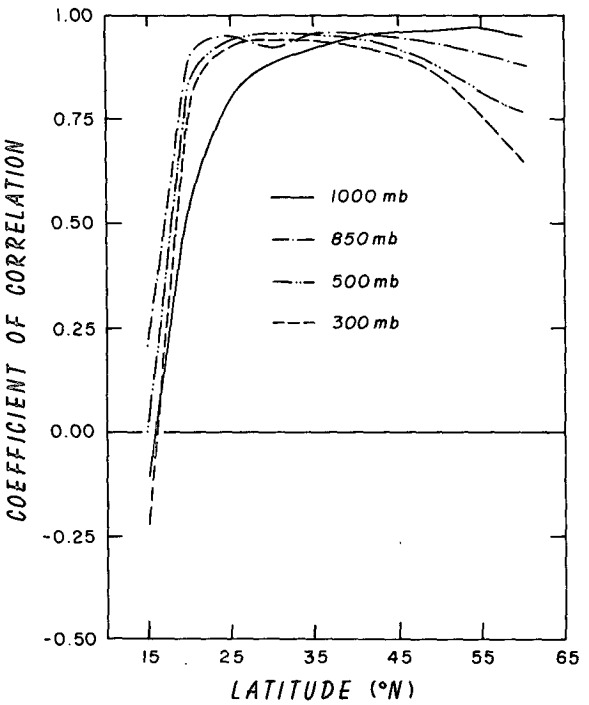

FIG. 1. Coefficient of correlation between the vertically integrated meridional eddy sensible heat flux from surface to a certain pressure level and the vertically integrated meridional temperature gradient as a function of latitude for several top pressure levels.

than 80% for pressure levels lower than 300 mb. It is quite evident, therefore, that Eq. (3.4) appears to be physically valid in midlatitudes where large-scale eddy transports are significant mechanisms in regulating the temperature distribution.

Using the same argument, we further postulate that the eddy transport of latent heat may be correlated with the water vapor mixing ratio gradient in the form

$$\int_0^z ([\overline{v'q'}] + [\bar{v}^*\bar{q}^*])\rho dz' = -K_3 \int_0^z \frac{\partial q}{\partial \lambda}\rho dz'. \quad (3.5)$$

We have also performed statistical analyses involving Eq. (3.5). The coefficients of correlation are not as good as in the temperature case ($\leqslant 50\%$). This indicates uncertainty in the water vapor mixing ratio data and insufficiency of its data spread to achieve a statistically meaningful correlation. Nevertheless, Eq. (3.5) seems to be physically adequate in performing climate sensitivity analyses.

Finally, we note that the meridional eddy transport of potential energy is much smaller than that of sensible and latent heat. For the climate numerical modeling, we may neglect its contribution. Thus, the large-scale horizontal eddy transport of the static energy may be summarized as follows:

$$\int_0^z ([\bar{v}^*\bar{E}^*] + [\overline{v'E'}])\rho dz' = -K_1 \int_0^z \left(\frac{\partial T}{\partial \lambda} + K_2\right)\rho dz' - K_3 \int_0^z \frac{\partial q}{\partial \lambda}\rho dz'. \quad (3.6)$$

Values of K_1, K_2 and K_3 as functions of latitude and height are depicted in Fig. 2 for reference. These K values are therefore specified as functions of height and latitude. In reality, however, they may vary with the temperature and temperature gradient. The dependence of K values on large-scale parameters and the incorporation of this dependence effectively and economically in climate modeling and feedback studies are certainly areas requiring further research and investigation. On examination of Eqs. (3.6) and (3.1), we see the resemblance of the two equations, namely, the use of the basic K-theory for turbulent transport. The horizontal transport, however, is expressed in terms of the integrated quantity with respect to height or pressure.

In a recent paper by Hoffert *et al.* (1983) which discussed a one-dimensional energy balance model, it was pointed out that the large-scale thermal diffusivity may be subject to the tropical evaporation constraint. An exact quantitative relationship has not been established, however. In the work of Peng *et al.* (1982), it was assumed that all horizontal transport in extratropical areas is due to the transient eddy which is parameterized using Stone's (1974) formulations. In addition, to account for mean circulation

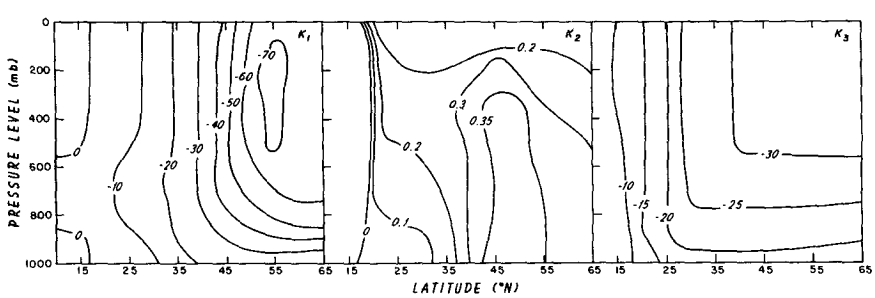

FIG. 2. Values of K_1 (m · Lat s^{-1}), K_2 (K Lat^{-1}) and K_3 (m · Lat s^{-1}) as functions of latitude and height defined in Eqs. (3.4) and (3.5).

in the tropics, they have included a parameterized Hadley circulation and estimated the latent heat release using Kuo's cumulus parameterization. As described in the preceding section, our approach is uniformly based on thermodynamic rather than dynamic principles. That is, horizontal transient and stationary eddy transports of both sensible and latent heat are parameterized utilizing the large-scale diffusion approximation in terms of the K-theory. This diffusion approximation was developed in terms of the integrated temperature and water vapor mixing ratio gradients. Furthermore, horizontal transports of latent and sensible heat by mean circulations were included in the model via the prescribed mean velocities.

c. *Surface flux*

In Eq. (2.7), we define the surface term R, which, from the surface energy budget point of view, must be associated with ocean transports. In order to evaluate this term, we require knowledge of the net radiation flux at the surface, which can be obtained from the radiation program, and the vertical surface flux. At the surface $\bar{w} = 0$, and since $[\bar{w}^*\bar{E}^*]$ is negligibly small, the vertical flux is basically represented by $\rho[\overline{w'E'}]$. Since the surface vertical flux transfer is related to temperature and water vapor mixing ratio gradients at the surface, it appears physically appropriate to assume that

$$\rho[\overline{w'E'}]|_{z\to 0} = c_1\left(\left|\frac{\partial T}{\partial z}\right| + \frac{L}{C_p}\left|\frac{\partial q}{\partial z}\right|\right)^{c_2}_{z\to 0}, \quad (3.7)$$

where c_1 and c_2 are certain constants which should depend on atmospheric conditions in terms of time and space scales. Strictly speaking, the surface flux parameterization should be based on boundary layer physics taking into account such factors as soil moisture, vegetation, ground water, ocean roughness, etc. However, in large-scale numerical modeling, parameterization of surface fluxes cannot be very detailed and complicated in view of the requirement of computational efficiency. For climate modeling applications, it appears physically appropriate to use the climatological surface energy budget data to derive the constants depicted in Eq. (3.7). In line with this objective, we utilize surface energy budget data listed in Sellers (1965) (who utilized earlier results of Budyko) and, more recently, in Budyko (1982), along with annual average temperatures and water vapor mixing ratios at 1000 and 950 mb provided by Oort and Rasmusson.

Figure 3 illustrates the sum of sensible and latent heat fluxes as a function of $(|\partial T/\partial z| + (L/C_p)|\partial q/\partial z|)|_{z\to 0}$ denoted as Γ in the graph, where $|\partial T/\partial z|$ is evaluated at 975 mb and $|\partial q/\partial z|$ is estimated from

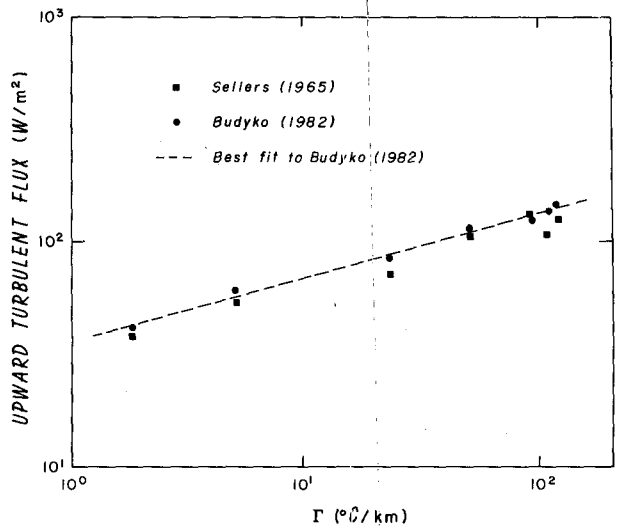

FIG. 3. The sum of surface upward sensible and latent heat fluxes derived by Sellers (1965) and Budyko (1982) versus Γ (=$[|\partial T/\partial z| + (L/Cp)|\partial q/\partial z|]|z\to 0$) obtained from Oort and Rasmusson (1971), where both gradient terms are zonally averaged values.

the difference of the water vapor mixing ratio and its saturation[1] value at 1000 mb. Both gradient terms are zonally averaged values. If $(\partial T/\partial z) + (L/C_p)(\partial q/\partial z) > 0$, the vertical flux is assigned a negative value and, therefore, it is downward. As is evident from this diagram, the total upward fluxes correlate well with the sum of the temperature and humidity gradients. The coefficients derived from the statistical analysis are $c_1 = 37$ and $c_2 = 0.276$. Thus, k_z values at the surface may be obtained from Eqs. (3.1) and (3.7). In climate sensitivity analyses, k_z in the constant flux layer is assumed to be independent of climate changes.

In the present study, we have determined the surface sensible and latent flux from climatological data in terms of surface temperature and humidity gradients. No direct dynamic factors such as frictional force and constant drag coefficient (Peng *et al.*, 1982) were employed in the parameterization, however.

4. Parameterization of various feedback mechanisms

a. *Humidity feedback*

Following the pioneering analysis carried out by Manabe and Wetherald (1967), we assume that the relative humidity r may be regarded as a constant in climate perturbation studies. The relative humidity is defined by

[1] Note that $L/C_p\partial q/\partial z$ denotes the latent heat transport gradient which is produced by the difference of saturated vapor density at the water surface and unsaturated vapor density in the air immediately above the water surface.

$$r = \frac{P_v}{P_v^*} = \frac{P_{v0}}{P_{v0}^*} = \text{constant}, \tag{4.1}$$

where P_v and P_v^* are the water vapor and its saturation pressure and P_{v0} and P_{v0}^* are corresponding values associated with the climatological temperature field.

Subject to the constant relative humidity assumption and utilizing the Clausius-Clapeyron equation, the mixing ratio in terms of climatological data may be expressed by

$$q = q_0 g(T), \tag{4.2}$$

with

$$g(T) = \exp\left[-\frac{L}{\tilde{R}}\left(\frac{1}{T_0} - \frac{1}{T}\right)\right]. \tag{4.3}$$

Thus, the horizontal and vertical humidity gradients may be expressed by

$$\left.\begin{aligned} \frac{\partial q}{\partial \lambda} &= \frac{\partial q_0}{\partial \lambda} g(T) + \frac{\partial g(T)}{\partial \lambda} q_0 \\ \frac{\partial q}{\partial z} &= \frac{\partial q_0}{\partial z} g(T) + \frac{\partial g(T)}{\partial z} q_0 \end{aligned}\right\}. \tag{4.4}$$

The second terms on the right in this equation are normally very small since vertical and horizontal gradients of $g(T)$ are small. Eq. (4.4) may then be incorporated into Eqs. (3.2), (3.6) and (3.7) to investigate the humidity feedback caused by variations of the temperature field.

b. *Ice-albedo feedback*

One of the input parameters in the solar radiation program is the surface albedo. Its distribution can be estimated from the known albedo values for various types of surfaces weighted by the fractional surface area employed in the numerical experiment. The latitudinal distribution of the surface albedo has been evaluated by a number of researchers (e.g., Sellers, 1965; Katayama, 1966; Robock, 1980). In order to parameterize the ice–albedo feedback to the temperature field, we require the relationship of the seasonal variation of the surface albedo, surface temperature and ice-covered area.

In this study, we propose a simple parameterization scheme using the statistical relationship between the surface albedo and surface temperature directly, without computing ice-covered areas. It would be desirable to employ annual surface albedo values to derive the surface albedo and surface temperature relationship. Unfortunately, such a data base does not exist. In a recent publication, however, Robock (1980) presented seasonal albedo values as functions of monthly surface temperatures. Using these values and monthly surface temperatures compiled by Oort and Rasmusson (1971) for a number of latitudes ranging from 5 to 85°N, we have attempted to derive their statistical relationships. On inspection and analysis of the variation of the ice–albedo pattern with respect to the latitude and surface temperature as depicted in Fig. 4, the

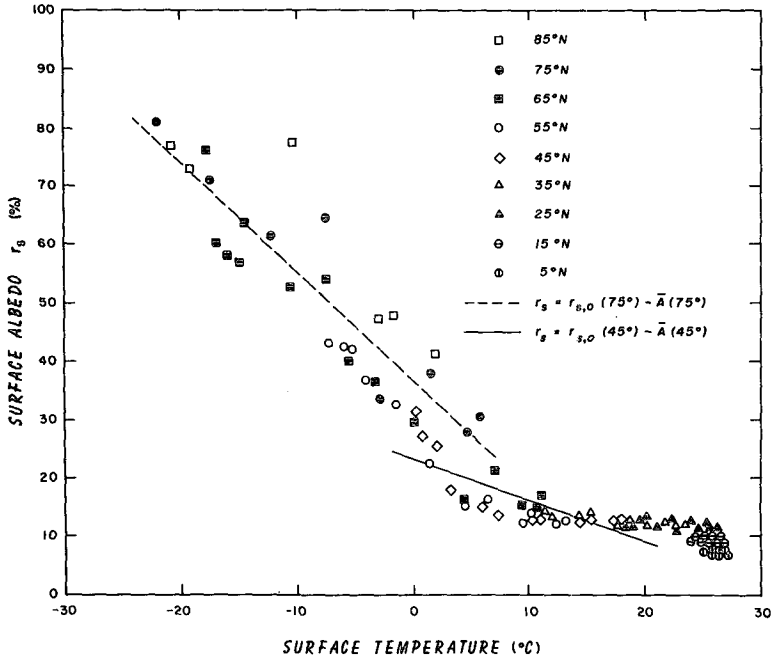

FIG. 4. The seasonal albedo values compiled by Robock (1980) as functions of the monthly surface temperatures provided by Oort and Rasmusson (1971) for several latitudes between 5 and 85°N. Also shown are results of empirical fitting at two different latitudes of 45 and 75°N. Note that $\bar{A} = A(T_s - T_{s0})e^{1-90°/\lambda}$.

following parameterized equations are derived to define the surface albedo:

$$\left.\begin{aligned} r_s(\lambda, T_s) &= r_{s0}(\lambda, T_{s0}) - A(T_s - T_{s0})e^{1-90°/\lambda}, \\ &\qquad\qquad \lambda \geq 30°\text{N} \\ r_s(\lambda, T_s) &= r_{s0}(\lambda, T_{s0}), \quad \lambda < 30°\text{N} \end{aligned}\right\}, \quad (4.5)$$

where $r_{s0}(\lambda, T_{s0})$ represents the climatological surface albedo value, T_{s0} is the climatological surface temperature and $A = 0.01875°\text{C}^{-1}$. In Eq. (4.5) when $\lambda \to 0°$, $r_s \to r_{s0}$ and when $\lambda \to 90°$, $r_s \to r_{s0} - A(T_s - T_{s0})$. Although the monthly surface albedo data presented by Robock (1980) differ somewhat from other data sources (e.g., Kukla and Robinson, 1980), the annual value $r_{s0}(\lambda, T_{s0})$ for each latitude is approximately the same from different surface albedo sources (Fig. 19, Robock, 1980). Moreover, it is evident that

$$\frac{\partial r_s}{\partial T_s} = -Ae^{1-90°/\lambda}. \quad (4.6)$$

Therefore, the sensitivity of the ice–albedo effect increases poleward. And since decreasing the surface temperature will increase the surface albedo, which in turn will further reduce the surface temperature due to additional reflection of solar fluxes, the ice–albedo feedback is clearly a positive mechanism. In Sellers's pioneering paper (1969), the planetary albedo is correlated with the surface temperature, i.e., $r = b + cT_s$ where b and c are empirical constants. Moreover, Sellers (1973) correlates the planetary albedo with surface albedo using a simple geometric ray-tracing technique. By carrying out analyses of $\partial r_s/\partial T_s = (\partial r_s/\partial r)(\partial r/\partial T_s)$, we find that the slope $A \sim 0.014°\text{C}^{-1}$ for $0.5 < r_s < 0.7$. Sellers's value, which does not account for the latitudinal dependence, is fairly close to the present result.

c. *Dynamic transport feedback*

In subsections 3a and 3b, we have presented parameterizations of the vertical and horizontal eddy transports in terms of temperature and mixing ratio gradients as shown in Eqs. (3.1) and (3.6). In addition, the vertical and horizontal mean transports denoted in Eq. (2.4) may be expressed as functions of temperature and mixing ratio in the forms

$$\rho[\bar{w}][\bar{E}] = \rho[\bar{w}]C_p\left(T + \frac{\phi_z}{C_p} + \frac{L}{C_p}q\right), \quad (4.7)$$

$$\int_0^z [\bar{v}][\bar{E}]\rho dz' = \int_0^z [\bar{v}]C_p\left(T + \frac{\phi_z}{C_p} + \frac{L}{C_p}q\right)\rho dz', \quad (4.8)$$

where the mean meridional and vertical velocities $[\bar{v}]$ and $[\bar{w}]$, respectively are taken from data provided by Oort and Rasmusson (1971). Thus, mean meridional and Hadley circulations are prescribed in the model. In view of Eqs. (3.1), (3.6), (4.7) and (4.8), it is evident that all the dynamic transport variations are now expressed in terms of temperature and water vapor mixing ratio.

Moreover, to investigate the deviation of horizontal dynamic transports from climatological values due to radiation perturbations, we express the change of integrated horizontal fluxes $\Delta\bar{F}_h$ defined in Eqs. (2.4) and (2.8) in the form

$$\Delta\bar{F}_h = -K_1\int_0^z \frac{\partial}{\partial\lambda}(T - T_0)\rho dz' - K_3\int_0^z \frac{\partial}{\partial\lambda}(q - q_0) \times \rho dz' + \int_0^z [\bar{v}]C_p\left[(T - T_0) + \frac{L}{C_p}(q - q_0)\right]\rho dz', \quad (4.9)$$

where the subscript 0 denotes climatological values. A similar expression may be written for the change of vertical fluxes. In climate perturbation experiments, the total (eddy plus mean) horizontal transport of sensible and latent heat will be a function of the variations of temperature and water vapor mixing ratio in the model.

5. Numerical solution to climatic perturbation

Since all the required parameterizations with respect to the IR and solar flux transfer and vertical and large-scale horizontal flux transports have been established, we may now rewrite the energy balance equations denoted in Eq. (2.8) in the form

$$-k_z\rho C_p\left(\frac{\partial T}{\partial z} + \gamma'\right) + F_{\text{IR}}(z, \lambda) = F_S(z, \lambda) - \tilde{B}(z, \lambda), \quad (5.1)$$

where we have separated the net flux term $F(z, \lambda)$ into the IR flux $F_{\text{IR}}(z, \lambda)$ and the solar flux $F_S(z, \lambda)$, and the last term is defined by

$$\tilde{B}(z, \lambda) = \rho[\bar{w}][\bar{E}]|_{z,\lambda} + \frac{1}{a\cos\lambda}\frac{\partial}{\partial\lambda}\cos\lambda\left\{\int_0^z [\bar{v}][\bar{E}]\rho dz - K_1\int_0^z\left(\frac{\partial T}{\partial\lambda} + K_2\right)\rho dz' - K_3\int_0^z \frac{\partial q}{\partial\lambda}\rho dz'\right\} + R(0, \lambda), \quad (5.2)$$

where the mean static energy $[\ddot{E}] = C_pT + Lq + \phi_z$. The surface term is now given by

$$-R(0, \lambda) = F_{\text{IR}}(0, \lambda) - F_S(0, \lambda) + c_1\left(\left|\frac{\partial T}{\partial z}\right| + \frac{L}{C_p}\left|\frac{\partial q}{\partial z}\right|\right)^{C_2}_{z\to 0}, \quad (5.3)$$

and the IR term is given by (Liou and Ou, 1983)

$$F_{\text{IR}}(z, \lambda) = \int_0^\infty \sigma T^4(z', \lambda)K(|z - z'|, \lambda)dz'. \quad (5.4)$$

The preceding equations constitute the two-dimen-

sional energy balance model. Integration of Eq. (5.1) from equator to pole and evaluating the net solar (E_S) and IR(E_{IR}) fluxes at the top of the atmosphere (i.e., $z \rightarrow \infty$), we find that $E_{IR} - E_S \approx 0.2 \times 10^{15} W$ for the Northern Hemisphere. This deficit is balanced by the interhemispheric transport by the atmosphere and ocean currents (see Fig. 11).

In order to solve Eq. (5.1) for the temperature field subject to Eqs. (5.2)–(5.4) we first postulate that the present climatic state will define the required $\tilde{B}$ [as given in Eq. (5.2)], which will produce the climatological temperature field of the earth–atmosphere system. Thus, on utilizing the climatological temperature, radiatively active gaseous profiles and the mean $\bar{v}$ and $\bar{w}$ fields, values for $\tilde{B}_0$ as a function of height and latitude may be obtained. Consequently, two terms on the right-hand side of Eq. (5.1) can now be considered constants with respect to the temperature. Subsequently, we may then solve Eq. (5.1) numerically for the temperature field using the small perturbation technique developed by Liou and Ou (1983). This experiment is referred to as the control run. In the control run, we tune the temperature field to within ~0.1 K accuracy of the climatological temperature field compiled by Oort and Rasmusson (1971). This gives us a consistent check on the model and it is the only tune-up process employed in model experimentations. In Section 6 we will illustrate comparisons of the computed eddy transports of sensible and latent heat and ocean transport with the available observed data.

Numerically, we may express the control run denoted by subscript 0 in the form

$$-k_z \rho C_p \left(\frac{\partial T_0}{\partial z} + \gamma_0' \right) + \int_0^\infty \sigma T_0^4(z', \lambda) K(|z - z'|, \lambda) dz' = F_{S,0}(z, \lambda) - \tilde{B}_0(z, \lambda). \quad (5.5)$$

The right-hand side, therefore, represents forcing terms which generate the climatological (i.e., steady-state) temperature field. Now, we will consider perturbations of the temperature field caused by variations of the CO_2 content or solar constant or cirrus radiative properties. Let the subscript 1 in the following equations denote the perturbed quantities and first consider only humidity and ice-albedo feedbacks. We then write

$$-k_z \rho C_p \left[\frac{\partial T_1^{(n)}}{\partial z} + \gamma_1'^{(n)} \right] + F_{IR,1}^{(n)}(z, \lambda) = F_{S,1}^{(n-1)}(z, \lambda) - \tilde{B}_0^{(n-1)}(z, \lambda), \quad n = 1, 2, \ldots, N, \quad (5.6)$$

where $\tilde{B}_0$ is prescribed in this experiment and the superscript n denotes the number of iterations. Once one of the radiatively active elements has changed, there will be a new distribution of solar fluxes in the atmosphere. This in turn will produce a new temperature distribution via the small perturbation technique mentioned previously. Subsequently, there will be new water vapor mixing ratios and surface albedo values which are expressed in reference to the perturbed temperature and climatological values discussed in Subsections 4a and 4b. Successive iterations may then be carried out until the temperature field is converged. Normally, iterations of about ten times are sufficient to converge the temperature field within ~0.1%.

Next, we consider the dynamic transport feedback. Let m denote the number of iterations in this part of the perturbation experiment and we write

$$-k_z \rho C_p \left[\frac{\partial T_1^{(N+m)}}{\partial z} + \gamma_1'^{(N+m)} \right] + F_{IR,1}^{(N+m)}(z, \lambda) = F_{S,1}^{(N+m-1)}(z, \lambda) - \tilde{B}_1^{(N+m-1)}(z, \lambda), \quad m = 1, 2, \cdots M, \quad (5.7)$$

where $\tilde{B}_1^{(N+m-1)}$ is computed via Eqs. (5.2) and (5.3). Normally, about 20 or so dynamic transport feedback iterations are needed to converge the temperatures within about 0.1%. Thus, $T_1^{(N+M)}$ will be the desired temperature when all three feedbacks are incorporated in the model experiment.

6. Model simulation results

a. Input parameters

The present model is intended for the Northern Hemisphere because of the availability of various data sources. In the model, the Northern Hemisphere is divided into nine latitudinal belts with a 10° equal partition. The atmosphere is scaled into 18 pressure levels. From the surface (~1000 mb) to 800 mb, an increment of 50 mb is used; an increment of 100 mb is employed up to the 100 mb level. Between 100 mb and 0.1 mb, which is considered to be the top, the atmosphere is divided into six layers with an increment in the logarithmic scale.

The required atmospheric profiles include pressure, height (or geopotential height), air density, temperature and water vapor, ozone and carbon dioxide densities. The mixing ratio of carbon dioxide is assumed to be 330 ppm. Except for the ozone density, which is taken from values provided by McClatchey *et al.* (1971), all other profiles are obtained from data compiled by Oort and Rasmusson (1971). Since the latter authors present the profiles up to 50 mb only, we again use the profiles of McClatchey *et al.* above this pressure level.

All the required IR emissivities and solar absorptivities for H_2O, CO_2, O_3 and H_2O–CO_2 bands have been documented in our previous papers (Liou and Ou, 1983; Ou and Liou, 1983). The solar constant is

assumed to be 1353 W m^{-2}.[2] The duration of daytime is 12 hours for the annual case, while the cosine of the solar zenith angle μ_0 is calculated from the equation relating the latitude, solar declination, hour angle and μ_0. The surface albedo used in the model has been discussed in the previous section.

Annual latitudinal distributions of the cloud type, base height, thickness and fractional cover are obtained by averaging the seasonal data presented by London (1957). Solar reflection and transmission values for these cloud types and IR emissivities for cirrus are parameterized utilizing the method previously described by Liou and Ou. Except for cirrus, all other cloud types are assumed to be blackbodies. In London's data, the cirrus thickness (9–12 km) is a constant with respect to latitude.[3] As a result, its IR emissivity is also a constant.[4] Variations of the solar transmission and reflection for optically thin cirrus are basically a result of solar zenith angle changes from the equator to the pole.

b. *Radiation budget at the top of the atmosphere*

Figure 5a shows the net downward solar fluxes at the top of the atmosphere computed from the present model. Solar fluxes generated from the present model agree closely with observed results presented by Stephens *et al.* (1981), except in the polar region where the present result is higher by about 10–20 W m^{-2}. The difference could be due to the uncertainty of the model parameters used for the polar region. The maximum difference in midlatitudes and tropics is less than 10 W m^{-2} which is within the uncertainty of the satellite data (Ellis, 1977).

The computed latitudinal distribution of net upward IR fluxes at the top of the atmosphere is shown in Fig. 5b. Comparisons are also made with observed results given by Stephens *et al.* (1981). Lower IR fluxes are observed in the equatorial region because of the persistence of convective clouds. The IR fluxes increase poleward to 15–20°N, where a maximum is shown due to low cloudiness in the subtropical high, and then decrease toward the arctic. The latitudinal difference in IR fluxes is ~10–20 W m^{-2}.

Figure 5c depicts the latitudinal distribution of net radiative fluxes at the top of the atmosphere. Comparison with the observed net radiative flux distribution depicted in the paper by Stephens *et al.* (1981) shows that differences are generally less than 20 W m^{-2}. Note that the radiation balance is positive ($F_S - F_{IR} > 0$, net heating) south of 35°N and negative

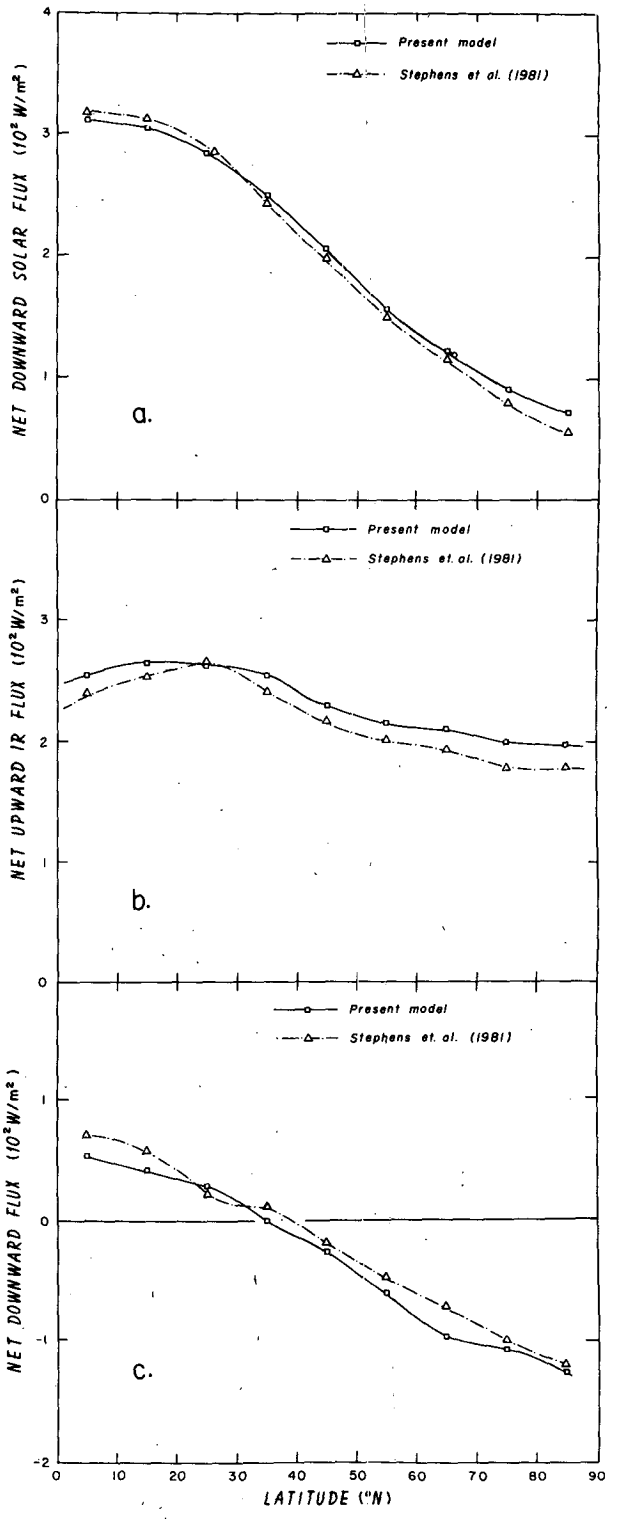

FIG. 5. (a) The net downward solar fluxes, (b) the net upward IR fluxes and (c) the net downward radiative fluxes at the top of the atmosphere as functions of latitude.

[2] This value is the standard solar constant issued by NASA in 1976. More recently, a value of 1373 W m^{-2} has been observed and proposed which is about 1.5% above the value used for model simulations in the present study.

[3] Unfortunately, London's data are the only available source for cloud climatology at this point in time. Recent studies by Short and Wallace (1980), Riehl and Miller (1978) and Warren and Thompson (1983) suggest that cirrus may be higher than London's data.

[4] Some point observations carried out by Griffith *et al.* (1980) indicated that tropical cirrus appear to be optically thicker than midlatitude cirrus.

(net cooling) north of 35°N. The maximum net flux is about 55 W m^{-2} within the lowest latitude belt, whereas the minimum is about -125 W m^{-2} within the polar belt (80–90°N). This meridional radiation flux difference will establish a steady-state energy flow such that excess radiative heat stored in low latitudes is transported to high latitudes through atmospheric and oceanic circulations. The relatively small, annual meridional temperature gradient observed is evidently the result of large-scale horizontal transports. If these transports were not accounted for, the tropical temperature would have been much higher, whereas the polar temperature would have been much lower.

c. *Surface energy balance*

Components of the surface energy balance are the net downward solar flux absorbed by the surface, the net upward IR flux, and upward sensible and latent heat fluxes. As noted in Eq. (5.3), the sum of these components is equal to $-R$, which represents the divergence of virtual oceanic transports. If $R < 0$, net heat fluxes transport out of the surface, and vice versa.

Figure 6a shows the latitudinal distribution of the net downward solar flux at the surface based on the present calculation. Comparisons with theoretical results presented by Stephens *et al.* (1981) illustrate close agreements. The maximum difference is within ~ 10 W m^{-2}. The decrease of solar radiation absorbed by the earth's surface with increasing latitude is clearly due to increasing mean annual solar zenith angle and surface albedo which effectively reduces sunlight absorbed by the surface.

Figure 6b shows the latitudinal distribution of net upward infrared fluxes at the surface. In low latitudes, our results are higher than those of Stephens *et al.* (1981) by about 8–10 W m^{-2}. It was suggested by Stephens *et al.* that low IR flux values in low latitudes are justified because the water dimer absorption in the 8–12 μm window is included in the calculation. Note that the present program also included the 8–12 μm window water dimer absorption in the calculation. Actual measurements of IR fluxes over the tropics, such as those presented by Ellingson and Gille (1978), reveal that surface net IR fluxes are on the order of 50–70 W m^{-2}. Low surface IR fluxes in the tropics derived in this study appear to be in agreement with observations.

Figure 6c shows the surface net downward radiative flux. Estimates of Budyko (1982) and Sellers (1965) are also depicted in the diagram for comparison purposes. Our results generally agree well with all others and they all show a general trend of the decrease of the net radiative flux with increasing latitude. Positive net downward radiative fluxes at the surface (except in near-polar regions) imply that net upward fluxes of sensible plus latent heat are needed to maintain the surface energy balance. The role of the virtual ocean transport is to relax the excess radiative flux absorbed in the tropics and to transport it to high-latitude regions.

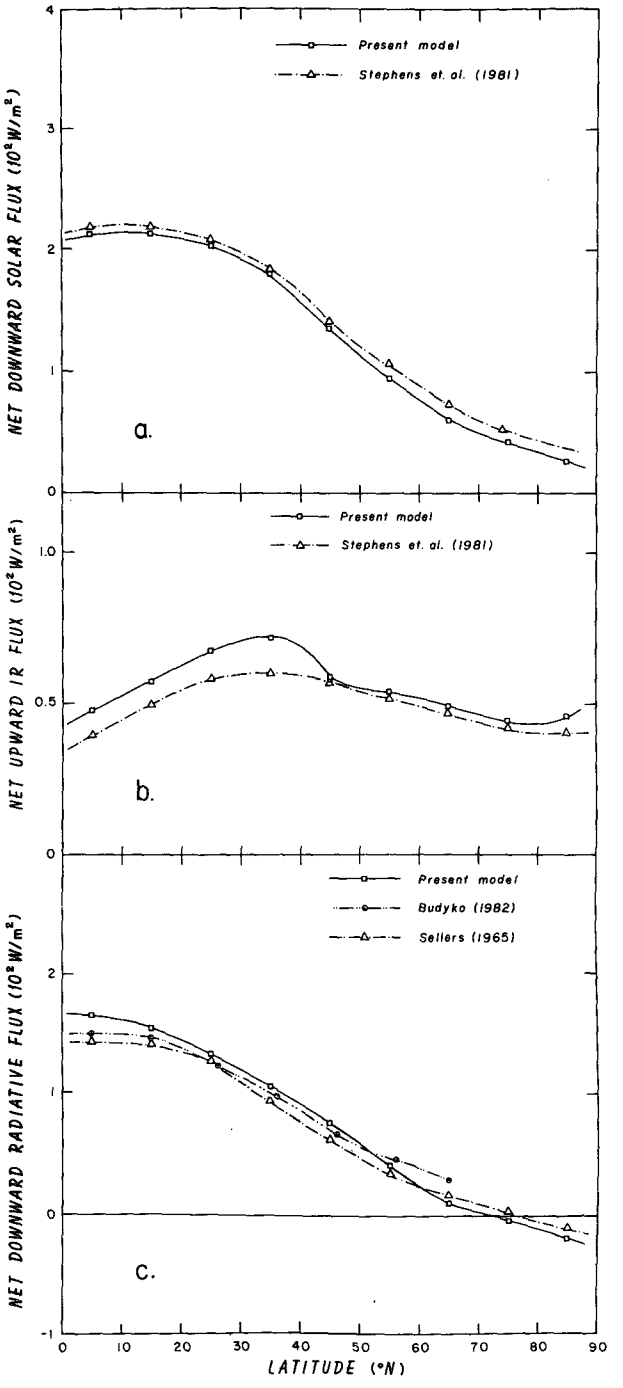

FIG. 6. As in Fig. 5 but for the surface.

Finally, Fig. 7 shows the model-generated latitudinal distribution of upward latent plus sensible heat fluxes at the surface. Also depicted for comparisons are results from Budyko (1982), Sellers (1965) and Oort and Vonder Haar (1976). These results for the tropical region differ by about 50 W m^{-2}. Our results, however,

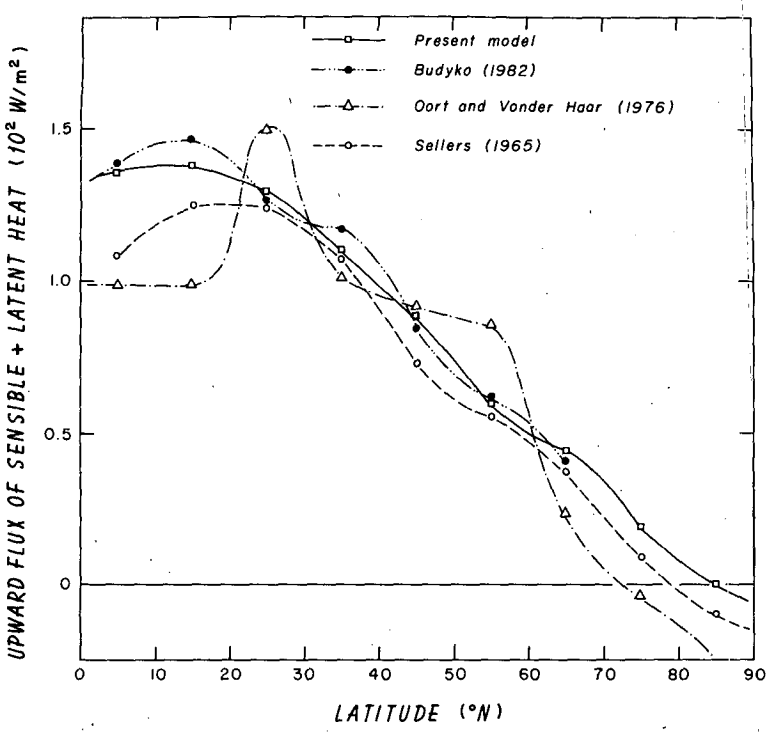

FIG. 7. The latitudinal distribution of the upward sensible plus latent heat fluxes at the surface.

agree closely with Budyko (1982) and Sellers (1965). The discrepancy in the tropics is mainly due to the fact that the estimated vertical eddy transport is subject to large uncertainties. As pointed out by Riehl (1982), a large fraction of the vertical transport takes plaee through the mechanism of cumulus formations which occupy only about 3–4% of the total tropical area. For this reason, it is very difficult to quantify the vertical transport based on data obtained from limited observational points. Note that Oort and Vonder Haar's results were obtained by subtracting the flux divergence of the oceanic transport from surface radiative balance values given by Sellers. The former value was derived from satellite radiation budget data. Also, note that their data curve shows oscillations about the values estimated by other workers. The vertical flux in the tropics is on the order of 100–150 W/m^2, and decreases monotonically with increasing latitude to about zero at the pole. This is in line with the results depicted in Fig. 6c where a net downward radiative flux is seen in a large portion of the Northern Hemisphere.

d. Dynamic transport

To illustrate the significance of large-scale horizontal transports, Fig. 8a shows temperatures obtained based on pure radiative balance computations. Under radiative equilibrium we see that the tropical surface temperature is well above 330 K, whereas temperatures as low as 200 K are observed in the arctic. We then incorporate the vertical eddy transport in the computation of thermal equilibrium temperatures. Results are shown in Fig. 8b. It is clear that the vertical eddy flux reduces the surface temperature somewhat so that the lapse rate becomes smaller and, therefore, the meridional temperature gradient is greatly reduced. However, in comparison with the climatological temperature field depicted in Fig. 11c, the tropical surface with a temperature of ~310 K is still too warm while the arctic is too cold (~210 K). Clearly, the horizontal transport must be accounted for in order to generate thermal equilibrium temperatures close to observed data.

Figures 9a and b show the latitudinal distribution of the flux divergence (R) of the virtual oceanic transport and its meridional transport rate (Φ_0) respectively. Since $R = d\Phi_0/dA$, where $dA = a^2 \cos\lambda d\lambda$, the poleward oceanic transport rate at a given latitude is given by

$$\Phi_0(\lambda) = \Phi_0(0) + \int_0^{\lambda} R(0, \lambda) a^2 \cos\lambda d\lambda, \quad (6.1)$$

where $\Phi_0(0)$ is the oceanic transport rate at the equator. The present results are compared with estimates given by Budyko (1982), Sellers (1965), Oort and Vonder Haar (1976) and Brian and Lewis (1979). In the case of the flux divergence, our results show agreements with other estimates except those of Oort

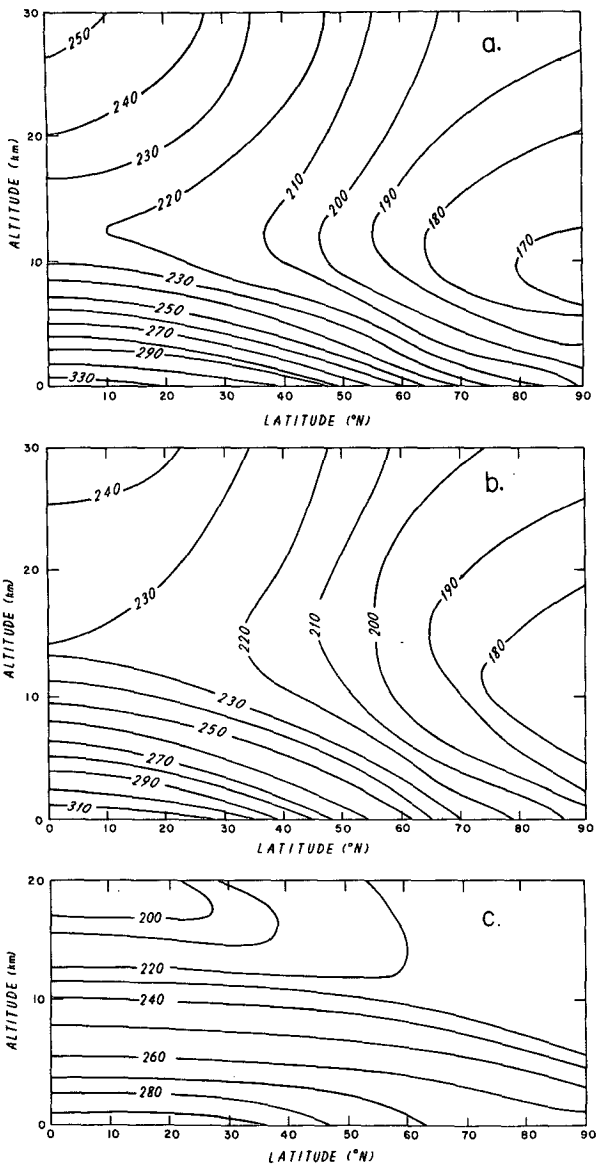

FIG. 8. The latitude-height temperature fields obtained based on (a) pure radiative equilibrium, (b) radiative plus vertical turbulent equilibrium and (c) observed data (Oort and Rasmusson, 1971).

and Vonder Haar (1976). As stated above, a smoothing process applied to their curve would make it closer to other estimates. Our flux divergence values in the tropics are higher, presumably due to higher surface net radiative fluxes (Fig. 6c). On the other hand, in the arctic, our results are lower than available estimates. It is possible that we may have overestimated the vertical transport in that area. In Fig. 9b, depicting the meridional transport rate, we see a large discrepancy in the estimated poleward transport between 5 and 70°N among various researchers. Vonder Haar and Oort (1973) have discussed uncertainty involved in estimating the poleward oceanic heat transport. Using the statistical sampling theory, they determined root-mean-square errors incurred in estimating the radiative balance at the top of the atmosphere from satellite data and poleward atmospheric heat transports, from which the oceanic transport was estimated. The vertical bars in Fig. 9b represent their estimated uncertainty distribution. In the tropics, the magnitude is on the order of 10^{15} W and it decreases gradually poleward. Thus, it appears that if poleward oceanic transport estimates are within vertical bars, these estimates may be considered reasonable. Note that all the estimates show maxima between 30 and 15°N.

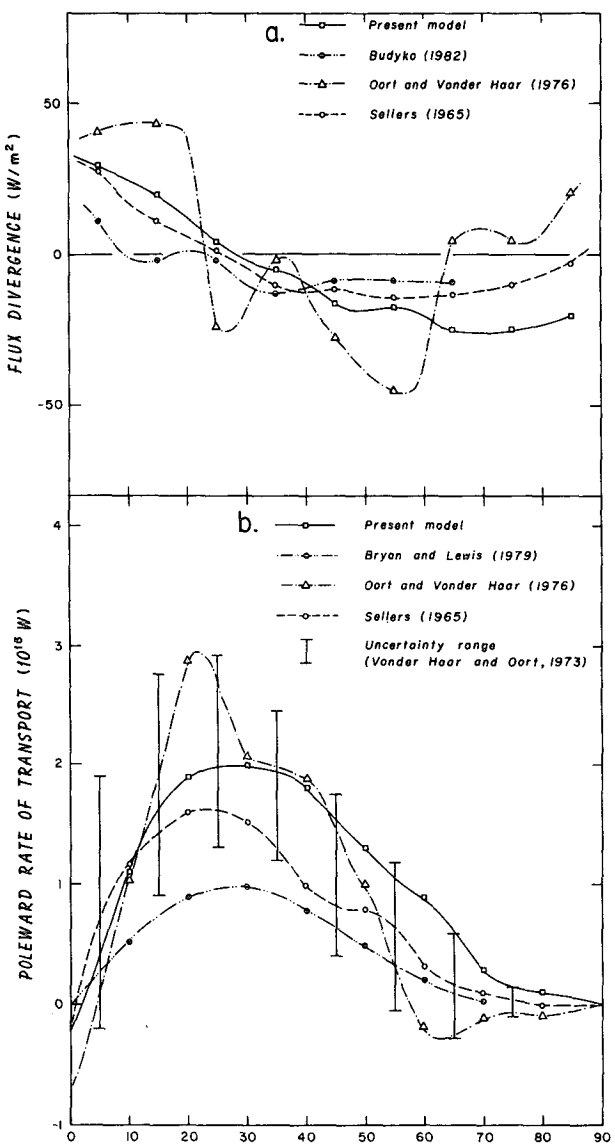

FIG. 9. The latitudinal distribution of the model-generated virtual oceanic transport in terms of (a) the flux divergence and (b) the poleward rate of transport along with other estimates of the ocean transport.

Model generated latitudinal distributions of the flux divergence (F_H) of the atmospheric heat transport and its corresponding poleward transport rate (Φ_A) are shown in Figs. 10a and b respectively. Here F_H is defined by

$$F_H = \frac{1}{a\cos\lambda}\frac{\partial}{\partial\lambda}\cos\lambda\int_0^\infty F_h(z',\lambda)dz'.$$

where F_h is defined in Eq. (2.4). Since $F_H = d\Phi_A/dA$, the poleward transport rate is given by

$$\Phi_A(\lambda) = \Phi_A(0) + \int_0^\lambda F_H(\lambda)a^2\cos\lambda d\lambda, \quad (6.2)$$

where $\Phi_A(0)$ denotes the atmospheric transport rate at the equator. The present results are compared with estimates provided by Sellers (1965) and Oort and Vonder Haar (1976). Our results agree with those of Sellers (1965), especially north of 35°N where differences are less than 10 W m^{-2}. The flux divergence is positive south of 35°N, signifying that there is an energy loss due to poleward heat flow out of this area. For this reason, the area with heat loss is characterized by a gradual increase in the poleward transport rate, whereas the reverse is true for the area with heat gain. The present model and the results of Sellers show that the maximum of the transport rate occurs at 40°N.

Finally, we construct a schematic latitudinal distribution of energy balance based on the present model-generated results. The upper and lower boxes in Fig. 11 represent, respectively, the atmosphere and the ocean (the land is excluded because of its relative insignificance in the role of heat transfer). $F(\infty)$ and $R(0)$ denote the net fluxes at the top of the atmosphere and the surface respectively. The two horizontal transport values Φ_A and Φ_0 depicted in the diagram were obtained from Eqs. (6.1) and (6.2). From this diagram, we see that south of 40°N the earth–atmosphere system receives a net flux of 5.5×10^{15} W. However, north of 40°N, the earth–atmosphere system emits 5.7×10^{15} W. Thus, a deficit of 0.2×10^{15} W of radiative flux is observed for the Northern Hemisphere. This deficit is balanced by the sum of the cross-equator transport, which is also 0.2×10^{15} W in the poleward direction.

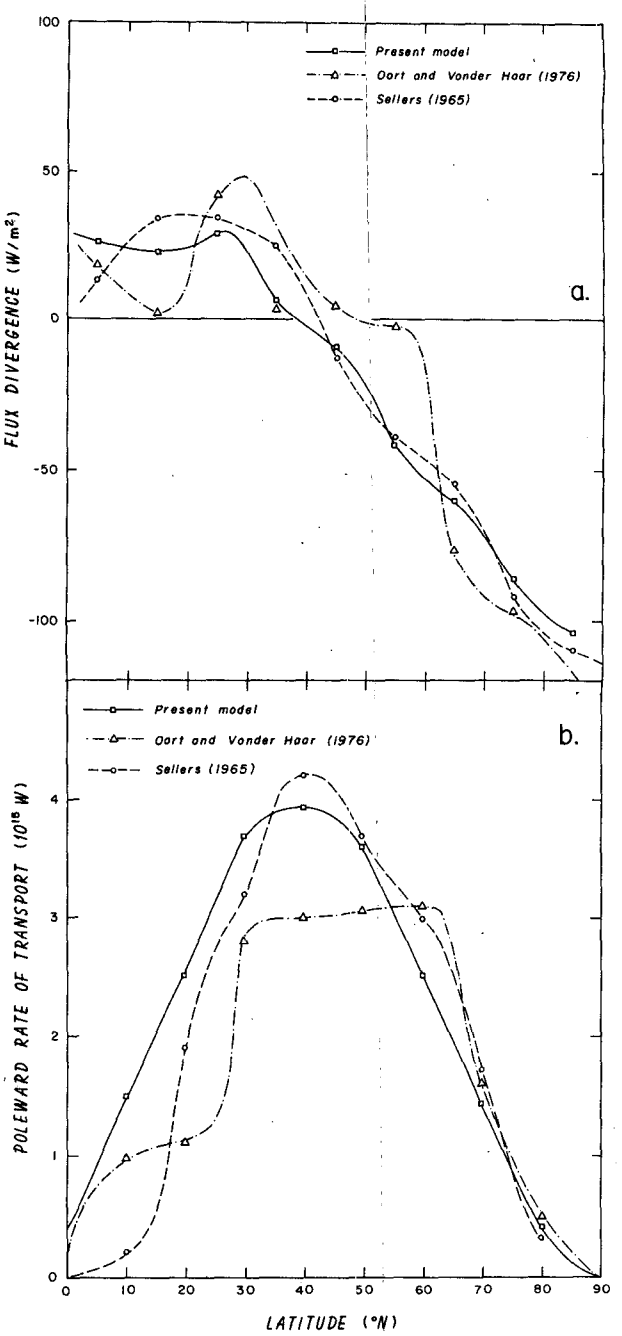

FIG. 10. As in Fig. 9 but for atmospheric transport.

e. *Thermal response to doubling of CO_2 and increase of solar constant*

To further check the validity of the present model, we performed experiments on the thermal responses to doubling the CO_2 and increasing the solar constant by 2%. We then compared our results with those presented by Wetherald and Manabe (1975) and Manabe and Wetherald (1980) who used general circulation models to perform sensitivity analyses.

Figure 12 shows the distribution of the temperature increase in the latitude–height domain due to doubling of the CO_2 concentration when all three feedbacks were considered in model simulations. The present results agree pretty closely with those presented by Manabe and Wetherald (1980). In the tropics, the surface temperature increase is about 2°C and it increases upward due to the additional latent heat release. The surface temperature change becomes rather large toward the polar region due to the ice–albedo feedback. However, this large increase due to doubling of CO_2 is confined to the low region because

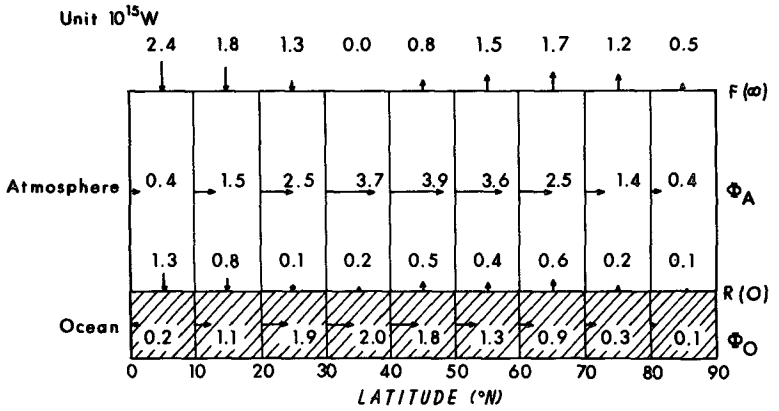

FIG. 11. The schematic latitudinal distribution of energy balance based on the model-generated results, where the cross-equator transports are obtained from the residual of the hemispheric integration of the respective flux divergence.

of the lack of strong convective activities to carry this excess heating upward. In the stratosphere, cooling effects are observed because of the requirement of radiative equilibrium under which absorption of solar fluxes by ozone remains the same, but the increase in IR emissivity to space due to CO_2 doubling leads to the decrease of stratospheric temperatures (Manabe, 1983). However, the cooling produced from our experiments is relatively small, compared to that presented by Manabe and Wetherland (1980). This is probably due to the difference in computing CO_2 emission and absorption.

In addition, we compared the meridional transport gradient of the moist static energy $\Delta\Phi_A$ as a function of latitude computed from the present model with that presented by Manabe and Wetherald (1980). It is quite evident from Fig. 13 that the present two-dimensional result is in excellent agreement with the result derived from a more sophisticated general circulation model. The positive increase of $\Delta\Phi_A$ south

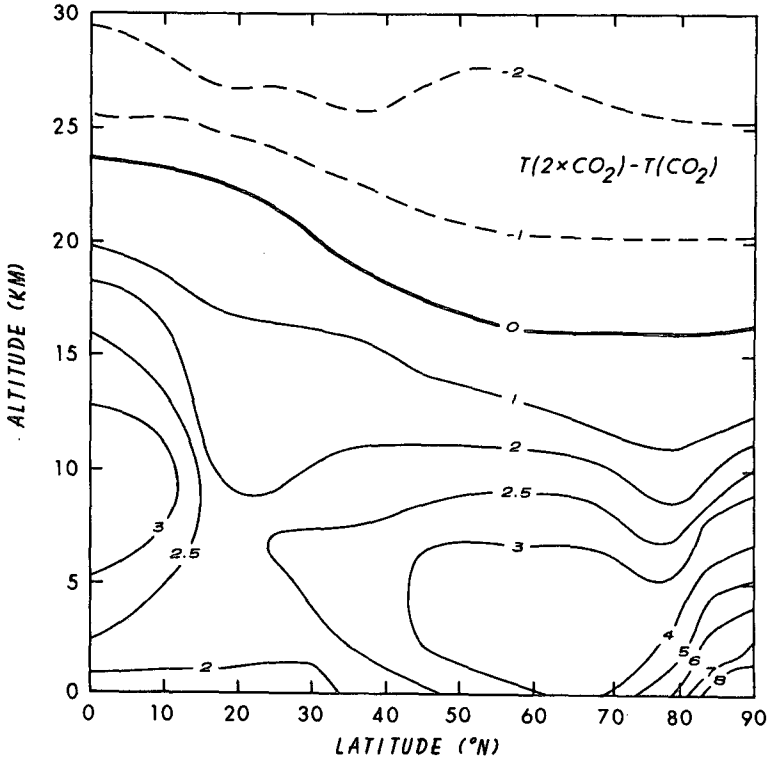

FIG. 12. The latitude–height distribution of the temperature change due to the doubling of CO_2 with all three feedbacks taken into consideration.

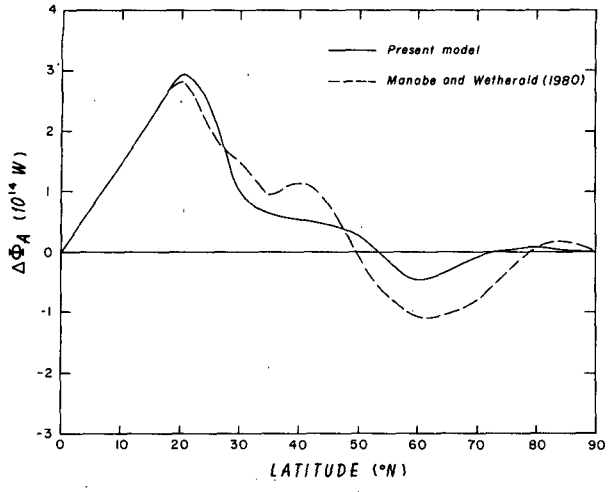

FIG. 13. The latitudinal distribution of the change in the meridional transport rate of the moist static energy, $\Delta\Phi_A$, due to doubling of CO_2. The dashed line is the result presented by Manabe and Wetherald (1980).

of 50°N is primarily caused by the large abundance of moisture in the tropics which is transported to high latitudes to reduce the large humidity gradient. Because of the temperature increase in polar regions, the poleward transport of sensible heat is gradually reduced so that $\Delta\Phi_A$ becomes negative between about 50 and 70°N.

Finally, we effected sensitivity model experiments with respect to the increase of solar constant and compared our results with those presented by Wetherald and Manabe (1975). Shown in Fig. 14 is the distribution of temperature increase due to the increases of solar constant by 2%. Increase of the temperature by about 3–4°C is seen in the troposphere and is especially evident in the tropics and midlatitudes. Owing to the ice-albedo feedback, as much as a 5–6°C temperature increase is observed in the polar boundary layer. These features are in general agreement with those obtained by Wetherald and Manabe (1975). However, in the tropical lower stratosphere, our result shows a larger warming as compared with that presented by Wetherald and Manabe. We suspect that this difference may well be a result of different gaseous absorptivities used in the solar transfer program. In summary, and in light of these comparisons, it appears that the present two-dimensional radiation–turbulence model performs quite satisfactorily with respect to the effects of the variations of internal (CO_2) and external (solar constant) components on the temperature field of the earth–atmosphere system.

7. Model sensitivity to variations in cirrus radiative properties

a. Temperature structure

It has been recognized that clouds, which constantly cover ~50% of the global sky are the most important regulators of the radiation balance of the earth–atmosphere system. While clouds reflect a significant portion of incoming solar fluxes, clouds also trap the outgoing thermal infrared fluxes emitted from the earth's surface and lower troposphere. The relative influence of the solar albedo effect versus the IR greenhouse effect determines the gain or loss of radiative energy during a specific climate change which leads to warming or cooling of the earth–atmosphere system. These two effects on the local scale obviously depend on both the specific earth–atmosphere conditions under which the clouds are embedded and their geometrical configuration and physical composition.

Clouds composed of water droplets are generally optically thick because of high droplet concentrations and therefore it is physically appropriate to assume these clouds to be blackbodies in the thermal infrared region. Even a thin stratus cloud with a thickness on the order of a few hundred meters may be considered to be a blackbody, to a good approximation. It would appear, therefore, that the solar albedo effect in the case of water clouds will produce greater variabilities of the radiative budget of the atmosphere, due to changes in the cloud vertical liquid water content. In addition, it has been shown by a number of numerical experiments employing a one-dimensional radiative and convective model that low and middle clouds will produce cooling effects because of the large solar opacity of these clouds (Manabe and Strickler, 1964; Manabe and Wetherald, 1967; Stephens and Webster, 1981; Liou and Gebhart, 1982).

On the other hand, high-level clouds, which contain

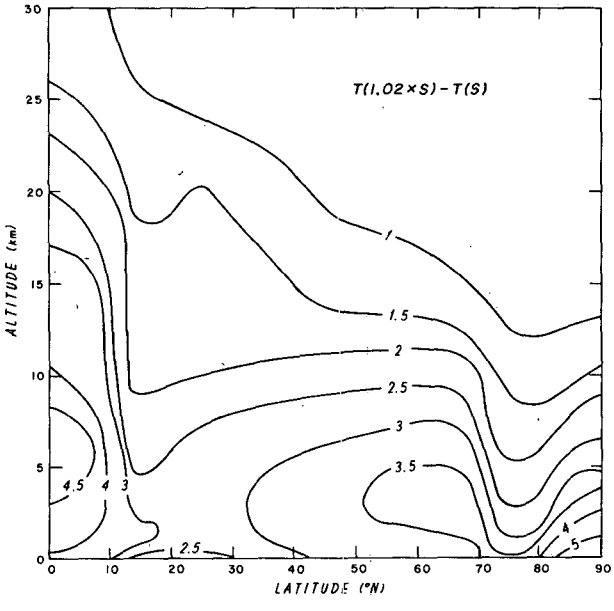

FIG. 14. The latitude–height distribution of the temperature increase due to a 2% increase of the solar constant with all three feedbacks considered.

a significant amount of large, nonspherical ice crystals with low concentrations (see, e.g., Heymsfield, 1975), are normally optically thin and nonblack. Owing to their high location in the atmosphere and low reflectance of the incoming solar fluxes, the presence of cirrus will lead to a general warming effect. This has been demonstrated in the paper by Liou and Gebhart employing a one-dimensional model. However, one of the fundamental parameters that will affect the radiative budget of the atmosphere is the cirrus radiative properties, including the solar reflections (albedo) and IR emissivity. These two basic radiative parameters are interrelated through the vertical ice content and the position of the sun. In this section, we wish to investigate the influence of the cirrus radiative properties on the temperature structure using the present two-dimensional radiation–turbulence climate model.

The cirrus radiative properties for both solar and IR spectra are functions of the cloud height, liquid water/ice content, particle size distribution, temperature, solar zenith angle and particle number concentration. Liou and Wittman (1979) utilized the liquid water/ice content and solar zenith angle as two prime independent variables in parameterizing the radiative properties of cirrus. Based on their polynomial expansions in terms of these variables, Fig. 15 shows the relationships between the solar reflectance and/or transmittance and IR emissivity, using the cosine of the solar zenith angle μ_0 from 0.1–0.8, a range applicable to all latitudes in annual climate modeling. The vertical dashed line at $\epsilon_0 = 0.47$ represents the cirrus IR emissivity determined from climatology data. To the left of this line, the solar reflectance and transmittance decreases and increases, respectively, with respect to smaller IR emissivities. To the right of this line, the solar reflectance also increases gradually for ϵ up to ~0.9. However, when the IR emissivity approaches unity, the solar reflectance (transmittance) increases (decreases) drastically. Thus, for a thin cloud (small emissivity), $\partial r_s/\partial\epsilon \ll 1$, while for a thick cloud (close to black), $\partial r_s/\partial\epsilon \gg 1$, where r_s is the solar reflectance. The quantity $\partial r_s/\partial\epsilon$ is related to the competition between the solar-albedo and greenhouse effect. Assuming that the changes in the emitted IR flux $F_{IR}(\infty)$ and the absorbed solar flux $F_S(\infty)$ are due solely to the perturbation in cirrus radiative properties, then $dF_{IR}(\infty)$ and $dF_S(\infty)$ should be functions of $d\epsilon$ and dr_s respectively.

In Fig. 15, we have related the solar reflectance and IR emissivity with cirrus vertical ice content in units of g m^{-2} used in this study. For the standard IR emissivity of 0.47, the corresponding ice content is ~5.7 g m^{-2}. In radiative transfer problems, it is convenient to use the optical depth to represent the opacity of clouds. Since the optical depth depends on the incident wavelength, it is difficult to derive a broadband optical depth associated with the IR emissivity and solar reflectance presented in this study.

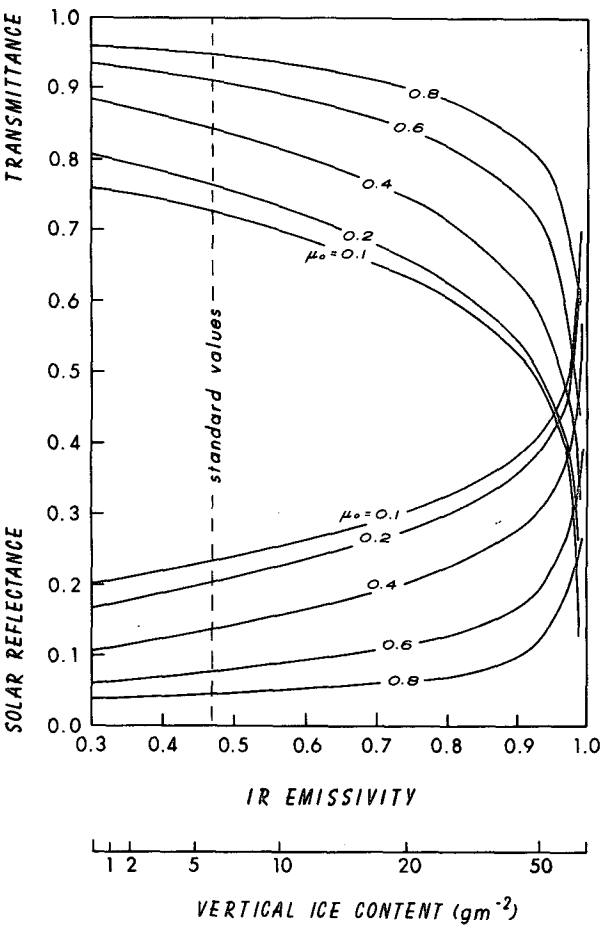

FIG. 15. The relationships between the solar reflectance/transmittance and IR emissivity for cirrus; μ_0 denotes the cosine of the solar zenith angle. The vertical dashed line at $\epsilon_0 = 0.47$ represents the cirrus IR emissivity determined from climatology data.

For a visible wavelength of 0.55 μm, the optical depth computed for cirrus with a thickness of 1.7 km and a vertical ice content of 5.7 g m^{-2} is about 0.5.

Quantitative demonstration of the relative importance of the albedo and greenhouse effects with respect to the cirrus IR emissivity and solar reflectance on the temperature structure is depicted in Fig. 16. This figure shows the latitude–emissivity contour map of the surface temperature change relative to the reference field. The magnitude of the change is small (±2°C for $0 < \epsilon < 0.9$) in the tropics, but rather large in the polar region due to the amplification effect of the albedo feedback. The large cooling in the arctic for the low cirrus amount is in accord with our daily experience that during winter nights, the surface temperature under a relatively clear sky condition will be much colder than that under cirrus conditions. The dash-dot line in the graph represents the maximum temperature increase for a given latitude. This line represents the position at which the greenhouse effect is at a maximum.

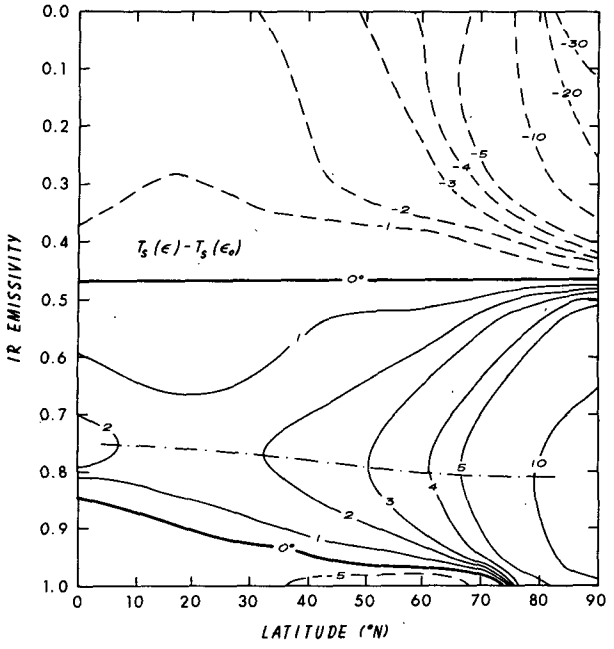

FIG. 16. The surface temperature changes as a function of latitude due to variations in the cirrus IR emissivity.

b. *The role of feedback*

Next, we wish to investigate the role of various feedbacks on the temperature perturbations due to changes in the cirrus radiative properties. In Figs. 17a and b, we show the percentage distribution of the surface temperature change caused by feedback coupling using $\epsilon = 0.32$ and $\epsilon = 0.57$, respectively, where the temperature change due to all three feedbacks is used as the basis. The surface temperature changes produced with no feedback vary from about 10% in the polar region to 60% in the tropics, with respect to those produced with all feedbacks included. The decrease in percentage poleward indicates that small internal perturbations may trigger large temperature changes due to the humidity and ice–albedo feedbacks. Furthermore, the humidity feedback is very pronounced in the tropics, while, as expected, the ice–albedo feedback is significant in the polar region.

On the other hand, the dynamic transport feedback, which includes the humidity transport, generally carries the heat from the surface to the atmosphere when surface temperature increases, thus reducing the percentage of temperature changes. When we compare the curves of the combined humidity and albedo feedbacks with all three feedbacks, we find the percentage of temperature changes exceeds 100% in the tropics and arctic, whereas it is less than 100% in middle-latitude regions. This demonstrates that the dynamic transport generally produces a negative feedback in the tropics and polar regions. This differs from the case when only dynamic transport feedback is considered in the model simulation. This occurs because when the only feedback is the dynamic transport, the meridional temperature change is almost negligible; therefore, only the vertical transport will affect the surface temperature variation. However, when both the humidity and albedo feedbacks are incorporated in the model, the meridional temperature gradient changes significantly so that the horizontal

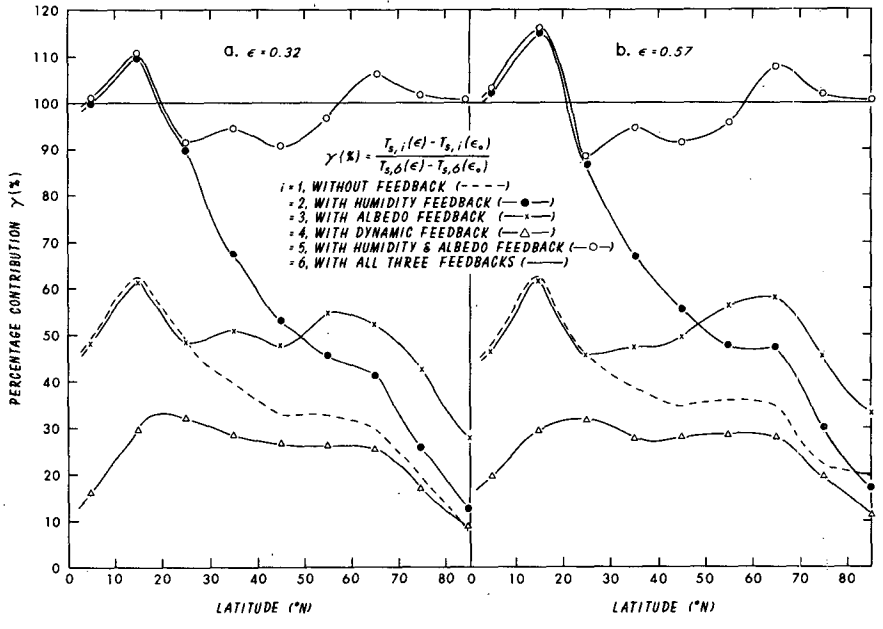

FIG. 17. The percentage contribution of the surface temperature change with respect to various feedback combinations due to changes in the cirrus IR emissivity. Left and right diagrams are for $\epsilon = 0.32$ and 0.57, respectively. The standard emissivity ϵ_0 considered is 0.47.

temperature adjustment will influence negatively the temperature change in the polar and tropical areas. Finally, we note that the behavior of the percentage distribution as a function of latitude is similar in both diagrams. This indicates that the relative importance of each feedback does not strongly depend on the radiative properties of cirrus within the context of the present model.

Finally, Figs. 18a and b illustrate the atmospheric temperature change caused by the decrease of cirrus IR emissivity from 0.47 to 0.32. Without the incorporation of various feedbacks, the temperature decrease due to the domination of the albedo effect when the IR emissivity decreases by 0.15 is generally less than 1°C. However, with all the feedbacks included in the experiment, the polar surface temperature is decreased significantly by as much as 10°C. Even in the tropics, the humidity feedback leads to a decrease of tropospheric temperatures on the order of ~2°C. We have also carried out experiments by increasing cirrus IR emissivity from 0.47 to 0.57. Results of temperature perturbations with and without feedbacks follow the foregoing patterns except with *positive* temperature increases.

8. Conclusions

In this paper, we have developed a two-dimensional radiation–turbulence climate model, which is based on the thermodynamic energy balance between radiation and vertical plus horizontal dynamic transports. In essence, this model is a logical extension of the semi-two-dimensional radiative–turbulent model developed previously by Liou and Ou (1983). Specifically, the model isolates terms related to dynamic transports of the moist static energy as the mean, transient eddy and stationary eddy components in both horizontal and vertical directions as well as ocean transports.

In the present model, the vertical eddy transport is parameterized utilizing the K-theory in turbulence. A counter-gradient factor has been added to the gradient term to account for the existence of counter-gradient flow in the observational statistics. The vertically averaged meridional eddy transport is correlated with the vertically averaged meridional temperature or humidity gradient. The coefficient of correlation for sensible heat components is more than 80% in the midlatitude area for all vertical levels. Moreover, the upward sensible and latent heat components at the surface were combined and parameterized in relation to the sum of the surface temperature and humidity derivatives. This fitting is supported by observed statistics.

The humidity feedback effect was taken into consideration via a constant-relative-humidity assumption. The relative humidity field was prescribed based on climatology data. The ice–albedo feedback was incorporated through a prescribed empirical relationship between the surface albedo and surface temperature. The mean sensitivity was found to be 1.875×10^{-2} °C^{-1}, which was about an order of magnitude larger than the correlation between the planetary albedo and surface temperature (Golitsyn, 1983). In addition, the dynamic transport feedback was simulated by separating temperature- and humidity-dependent terms in the energy balance equation. Consequently, the change in the rate of the dynamic transport due to thermal and hydrological variations can be incorporated through these terms. The thermodynamic energy balance equation was solved in a manner similar to that presented by Liou and Ou. However, since various feedback effects have been included, an iterative approach was undertaken in which the same balance equation was successively solved in each iteration.

The radiation budget at the top of the atmosphere and the surface energy budget, both derived from the

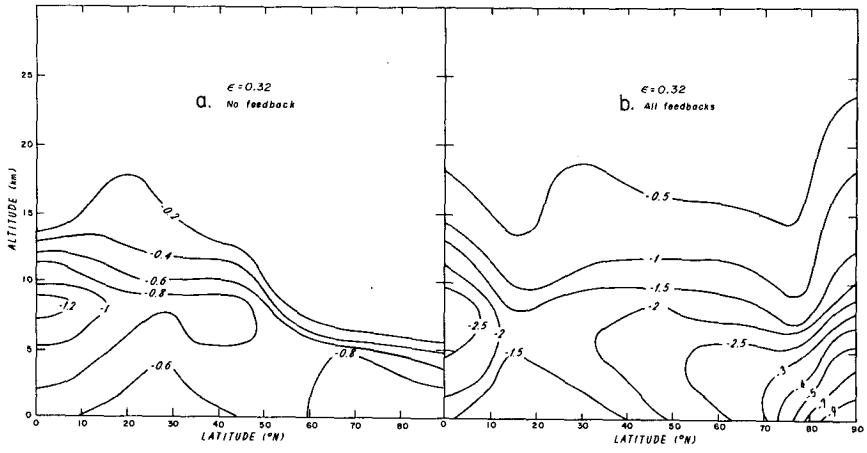

FIG. 18. The latitude–height distribution of the temperature change caused by a decrease of the cirrus IR emissivity from 0.47 to 0.32. (a) no feedback and (b) with all three feedbacks considered.

climatological field, agree well with satellite observed values. The vertically integrated transport of atmospheric moist static energy and the virtual oceanic transport were also verified against satellite-derived statistics. There is reasonable agreement between these sets of numerical values. To verify our model further, we performed experiments on doubling of CO_2 and the increase of the prescribed solar constant by 2%. Thermal responses from both experiments agree well with GCM results presented by Wetherald and Manabe (1975) and Manabe and Wetherald (1980).

Utilizing the present model we have investigated the climatic effect of changes in cirrus radiative properties. We first developed relationships between the solar reflectance (and transmittance) and IR emissivity based on parameterization equations derived by Liou and Wittman (1979) for cirrus. The climatological mean value for the cirrus IR emissivity was determined to be $\epsilon = 0.47$. We carried out a series of experiments involving latitude–height temperature responses to changes of cirrus IR emissivities employing values between 0 and 0.99, assuming that cirrus amount and cirrus height were fixed. It can be concluded that the greenhouse effect generally prevails, i.e., an increase in cirrus emissivity ϵ results in an increase in the surface temperature T_s. Only for optically thick cirrus with emissivity greater than about 0.8 is $\partial T_s/\partial \epsilon$ less than zero, implying that the albedo effect dominates.

The role of feedback mechanisms on the temperature perturbation caused by cirrus IR emissivity variations was investigated further. Qualitatively, the humidity feedback alone is most active in the tropics, while the ice–albedo feedback is extremely significant in the polar region. The combined effect of humidity and albedo is synergistic, especially in the arctic area where small internal perturbations may trigger large temperature changes. Feedback due to the dynamic transport generally carries sensible and latent heat from the surface to the atmosphere. As a result, the horizontal temperature and humidity gradients are reduced so that the change in horizontal transport is relatively small. When all three feedbacks are included, the dynamic transport becomes a negative feedback in tropical and polar areas, but a positive one in midlatitude regions. Finally, latitudinal distributions of the percentage of the surface temperature change due to various couplings of feedbacks, relative to that due to all three feedbacks, are shown to be extremely similar for the two emissivity values (0.32 and 0.57) used. This suggests that the relative importance of each feedback is dependent only slightly on cirrus radiative properties within the context of the present model.

Acknowledgments. This research has been supported by the Division of the Atmospheric Sciences, National Science Foundation under Grant ATM-81-09050. Sharon Bennett typed and edited several versions of the manuscript. Some of the reviewers' comments have led to significant improvement of the presentation of the paper.

REFERENCES

Branscome, L., 1983: A parameterization of transient eddy heat flux on a Beta-plane. *J. Atmos. Sci.*, **40,** 2508–2521.

Brian, K., and L. J. Lewis, 1979: A water mass model of the world ocean. *J. Geophys. Res.*, **84,** 2503–2517.

Budyko, M. I., 1982: *The Earth's Climate: Past and Future.* Academic Press, 307 pp.

Charlock, T. P., 1982: Cloud optical feedback and climate stability in a radiative–convective model. *Tellus,* **34,** 245–254.

Chou, M. D., L. Peng and A. Arking, 1982: Climate studies with a multi-layer energy balance model. Part II: The role of feedback mechanisms in the CO_2 problem. *J. Atmos. Sci.*, **39,** 2657–2666.

Clapp, P. F., 1970: Parameterization of macroscale transient heat transport for use in a mean-motion model of the general circulation. *J. Appl. Meteor.*, **9,** 554–563.

Deardorff, J. W., 1966: The counter-gradient heat flux in the lower atmosphere and in the laboratory. *J. Atmos. Sci.*, **23,** 503–506.

——, 1972: Theoretical expression for the counter-gradient vertical heat flux. *J. Geophys. Res.*, **77,** 5900–5904.

Ellingson, R. G., and J. C. Gille, 1978: An infrared radiative transfer model. Part I: Model description and comparison of observations with calculations. *J. Atmos. Sci.*, **35,** 523–545.

Ellis, J. S., 1977: Cloudiness: The planetary radiation budget and climate. Ph.D. dissertation, Colorado State University, 129 pp.

Golitsyn, G. S., 1983: Almost empirical approaches to the problem of climate, its variations and fluctuations. *Advances in Geophysics,* Vol. 25, Academic Press, 85–115.

Green, J. S. A., 1970: Transfer properties of the large-scale eddies and the general circulation of the atmosphere. *Quart. J. Roy. Meteor. Soc.*, **96,** 157–185.

Griffith, K. T., S. K. Cox and R. G. Knollenberg, 1980: Infrared radiative properties of tropical cirrus clouds inferred from aircraft measurements. *J. Atmos. Sci.*, **37,** 1077–1087.

Hartmann, D. L., and D. A. Short, 1980: On the use of earth radiation budget statistics for studies of clouds and climate. *J. Atmos. Sci.*, **37,** 1233–1250.

Herman, G. F., M. L. C. Wu and W. T. Johnson, 1980: The effect of clouds on the earth's solar and infrared radiation budgets. *J. Atmos. Sci.*, **37,** 1251–1261.

Heymsfield, A. J., 1975: Cirrus unicus generating cells and the evolution of cirroform clouds. Part I: Aircraft observations of the growth of the ice phase. *J. Atmos. Sci.*, **32,** 798–808.

Hoffert, M. I., B. P. Flannery, A. J. Callegari, C. T. Hsieh and W. Wiscombe, 1983: Evaporation-limited tropical temperatures as a constraint on climate sensitivity. *J. Atmos. Sci.*, **40,** 1659–1668.

Katayama, A., 1966: On the radiation budget of the troposphere over the northern hemisphere: I. Introduction. *J. Meteor. Soc. Japan,* **44,** 381–401.

Kukla, G., and D. Robinson, 1980: Annual cycle of surface albedo. *Mon. Wea. Rev.*, **108,** 56–68.

Liou, K. N., and G. D. Wittman, 1979: Parameterization of the radiative properties of clouds. *J. Atmos. Sci.*, **36,** 1261–1273.

——, and S. S. Ou, 1981: Parameterization of infrared radiative transfer in cloudy atmospheres. *J. Atmos. Sci.*, **38,** 2707–2716.

——, and K. L. Gebhart, 1982: Numerical experiments on the thermal equilibrium temperature in cirrus cloudy temperatures. *J. Meteor. Soc. Japan,* **60,** 570–582.

——, and S. S. Ou, 1983: Theory of equilibrium temperature in radiative–turbulent atmospheres. *J. Atmos. Sci.*, **40,** 215–229.

London, J., 1957: A study of the atmospheric heat balance. New York University, Final Rept., Contract AF19(122)-166, 99 pp.

Lorenz, E. N., 1979: Forced and free variations of weather and climate. *J. Atmos. Sci.*, **36**, 1367–1376.

Manabe, S., 1983: Carbon dioxide and climate change. *Advances in Geophysics*, Vol. 25, Academic Press, 39–82.

——, and R. Strickler, 1964: Thermal equilibrium of the atmosphere with a convective adjustment. *J. Atmos. Sci.*, **21**, 361–385.

——, and R. T. Wetherald, 1967: Thermal equilibrium of the atmosphere with a given distribution of relative humidity. *J. Atmos. Sci.*, **24**, 241–259.

——, and ——, 1980: On the distribution of climate change resulting from an increase in CO_2 content of the atmosphere. *J. Atmos. Sci.*, **37**, 99–118.

McClatchey, R. A., R. A. Fenn, J. E. Selby, F. E. Volz and J. S. Garing, 1971: *Optical Properties of the Atmosphere*, 3rd ed., AFCRL-72-0497.

O'Brien, J. J., 1970: A note on the vertical structure of the eddy exchange coefficient in the planetary boundary layer. *J. Atmos. Sci.*, **27**, 1213–1215.

Ohring, G., and P. Clapp, 1980: The effect of changes in cloud amount on the net radiation at the top of the atmosphere. *J. Atmos. Sci.*, **37**, 447–454.

Oort, A. H., and E. M. Rasmusson, 1971: *Atmospheric Circulation Statistics*. NOAA Prof. Paper 5, U.S. Department of Commerce, 323 pp. (DOC C 55.25:5).

——, and T. H. Vonder Haar, 1976: On the observed annual cycle in the ocean-atmosphere heat balance over the Northern Hemisphere. *J. Phys. Oceanogr.*, **6**, 781–800.

Ou, S. S., and K. N. Liou, 1983: Parameterization of carbon dioxide 15 μm absorption and emission. *J. Geophys. Res.*, **88**, 5203–5207.

Paltridge, G. W., 1980: Cloud-radiation feedback to climate. *Quart. J. Roy. Meteor. Soc.*, **106**, 895–898.

Peng, L., M. D. Chou and A. Arking, 1982: Climate studies with a multi-layer energy balance model. Part I: Model description and sensitivity to the solar constant. *J. Atmos. Sci.*, **39**, 2639–2656.

Potter, G. L., H. W. Ellaesser, M. C. MacCracken and F. M. Luther, 1978: Atmospheric statistical dynamic models, model performance: The Lawrence Livermore Laboratory zonal atmospheric model. *JOC Study Conf. on Climate Models: Performance, Intercomparison and Sensitivity Studies, GARP Publ. Ser.*, No. 22, WMO, Geneva, 852–871.

Riehl, H., 1982: *Climate and Weather in the Tropics*. Academic Press, 611 pp.

——, and A. H. Miller, 1978: Differences between morning and evening temperatures of cloud tops over tropical continents and oceans. *Quart. J. Roy. Meteor. Soc.*, **104**, 757–764.

Robock, A., 1980: The seasonal cycle of snow cover, sea ice and surface albedo. *Mon. Wea. Rev.*, **108**, 267–285.

Saltzman, B., and S. Ashe, 1976: The variance of surface temperature due to diurnal and cyclone-scale forcing. *Tellus*, **4**, 307–322.

Sasamori, T., and J. W. Melgarejo, 1978a: A parameterization of large-scale heat transport in mid-latitudes. Part I. Transient eddies. *Tellus*, **30**, 289–299.

——, and ——, 1978b: A parameterization of large-scale heat transport in mid-latitudes. Part II. Stationary waves and the Ferrel cell. *Tellus*, **30**, 300–312.

Sellers, W. D., 1965: *Physical Climatology*. The University of Chicago Press, 272 pp.

——, 1973: A new global climatic model. *J. Appl. Meteor.*, **12**, 241–254.

Short, D. A., and J. M. Wallace, 1980: Satellite-infrared morning-to-evening cloudiness changes. *Mon. Wea. Rev.*, **108**, 1160–1169.

Srivatsangam, S., 1978: Parametric study of large-scale eddy properties. *J. Atmos. Sci.*, **35**, 1212–1219.

Stephens, G. L., and P. J. Webster, 1981: Clouds and climate: Sensitivity of simple systems. *J. Atmos. Sci.*, **38**, 235–247.

——, G. G. Campbell and T. H. Vonder Haar, 1981: Earth radiation budgets. *J. Geophys. Res.*, **86**, 9739–9760.

Stone, P. H., 1974: The meridional variation of the eddy heat fluxes by baroclinic waves and their parameterization. *J. Atmos. Sci.*, **31**, 444–456.

——, and D. A. Miller, 1980: Empirical relations between seasonal changes in meridional temperature gradients and meridional fluxes of heat. *J. Atmos. Sci.*, **37**, 1708–1721.

Vonder Haar, T. H., and A. H. Oort, 1973: New estimate of annual poleward energy transport by Northern Hemisphere oceans. *J. Phys. Oceanogr.*, **3**, 169–172.

Wang, W. C., W. B. Rossow, M. S. Yao and M. Wolfson, 1981: Climate sensitivity of one-dimensional radiative-convective models with cloud feedback. *J. Atmos. Sci.*, **38**, 1167–1178.

Warren, S. G., and S. L. Thompson, 1983: The climatological minimum in tropical outgoing infrared radiation: Contributions of humidity and clouds. *Quart. J. Roy. Meteor. Soc.*, **109**, 169–185.

Wetherald, R. T., and S. Manabe, 1975: The effects of changing the solar constant on the climate of a general circulation model. *J. Atmos. Sci.*, **32**, 2044–2059.

——, and ——, 1980: Cloud cover and climate sensitivity. *J. Atmos. Sci.*, **37**, 1485–1510.